Sensitivity of the viscoplasticity of polycrystals to porosity and pore-to-crystal size ratio

Louis Védrine, Pascal Hagenmuller, Lionel Gélébart, Maurine Montagnat, Henning Löwe

Highlights

Sensitivity of the viscoplasticity of polycrystals to porosity and pore-to-crystal size ratio.

Louis Védrine, Pascal Hagenmuller, Lionel Gélébart, Maurine Montagnat, Henning Löwe

- The viscoplastic behaviour of synthetic porous microstructures is simulated using a crystal plasticity law.
- The stress exponent is sensitive to both solid fraction and intercrystalline surface area.
- The stress exponent is governed by the geometric frustration of the crystals caused by their neighbours.
- We clarify the transitions in viscoplastic behaviour with varying porosity, avoiding the need for additional mechanisms like grain boundary sliding.

Sensitivity of the viscoplasticity of polycrystals to porosity and pore-to-crystal size ratio.

Louis Védrine[a,*], Pascal Hagenmuller[a], Lionel Gélébart[b], Maurine Montagnat[a,c], Henning Löwe[a,d]

[a] *Université Grenoble Alpes, Université de Toulouse, Météo-France, CNRS, CNRM, Centre d'Etudes de la Neige, Grenoble, France*
[b] *Université Paris-Saclay, CEA, Service de Recherches Métallurgiques Appliquées, 91191, Gif-sur-Yvette, France*
[c] *Univ. Grenoble Alpes, CNRS, IRD, G-INP, IGE, Grenoble, France*
[d] *WSL Institute for Snow and Avalanche Research SLF, Fluelastrasse 11, Davos Dorf, 7260, Switzerland*

Abstract

Porous polycrystals are composed of pores and sintered crystals. Understanding their viscoplastic behaviour is crucial for predicting the mechanical performance of manufactured materials or the evolution of geological components. Their viscoplasticity intuitively depends on the shape of the solid matrix and how it is divided into individual crystals. Previous studies have primarily focused on limiting cases with low porosities or extreme pore-to-crystal size ratios. In this study, we use numerical full-field simulations on three-dimensional porous microstructures, combined with a crystal plasticity model, to explore how polycrystal viscoplasticity is affected by both geometric and crystalline structures. We use ice and its porous form, snow, as model materials. Our findings demonstrate that the homogenized strain rate $\dot{\epsilon}$ fits a power law of stress σ as $\dot{\epsilon} = \left(\frac{\sigma}{\sigma_0}\right)^n \text{s}^{-1}$ with σ_0 the reference stress and n the stress exponent. Notably, we show that the reference stress is determined solely by the geometric structure, while the stress exponent is influenced by both the geometric and crystalline structures. Specifically, the stress exponent is governed by the geometric frustration of the crystals caused by their neighbours, which modulates dislocation creep across different slip systems. By defining the pore-to-crystal size ratio as the area ratio between the crystal boundary and the free surface, we provide a coherent framework for understanding these interactions. This study clarifies the transitions in viscoplastic behaviour with varying porosity, avoiding the need for additional mechanisms and offering valuable insights into porous polycrystal viscoplasticity.

Keywords: Viscoplasticity, Porous Media, Polycrystal, Crystal plasticity, Fast Fourier Transform method

Introduction

This study investigates the viscoplastic behaviour of porous polycrystals, i.e., materials composed of pores and sintered crystals. Porous polycrystals comprise engineered materials, such as metallic powders and foams or polycrystalline nuclear fuels, and natural materials, such as snow. Thanks to the development of additive and powder-sintering techniques, manufactured porous polycrystals are increasingly used across various fields [1, 2, 3]. For instance, biomedical engineering, aerospace, automotive, naval, and defence industries benefit from their low specific weight and high energy absorption capacity [4, 5, 6]. Conversely, the manufacturing process or the industrial use of dense polycrystalline materials may lead to undesirable pores, negatively affecting their mechanical properties [7]. For instance, the accumulation of fission gases in nuclear fuels leads to porosity within the material and, possibly, to lower resistance to compression [8, 9]. Porous polycrystals are also among the natural materials commonly found on the Earth. In particular, the snow-ice continuum is an exemplary porous polycrystal characterized by sintered ice crystals of various sizes and textures [10], and a wide range of porosities from 90% for fresh snow, to around 50% for annual snow, to around 0% for dense polycrystalline ice on glaciers and polar ice sheets [11].

Under slow loading conditions and at temperatures close to their melting points, these materials exhibit viscoplastic deformations. This type of deformation typically occurs during the die compaction of metal powders [12, 13, 14, 15] and the natural settlement of snow [16, 17]. Viscoplasticity encompasses various deformation mechanisms. Depending on the crystalline structure of the materials and the nature of the applied loading (thermal, mechanical, or irradiative), the deformation mechanisms can either be dislocation creep (commonly referred to as intra-crystalline deformation) [18], grain boundary sliding (commonly referred to as intercrystalline deformation)[19], as well as mixed-induced thermal and irradiation-induced creep [20]. These mechanisms occur at the crystal scale and are highly dependent on the microstructure geometry or the crystal orientation [21].

Porous polycrystals are characterized by a dual structure comprising geometric features, i.e. the shape of the solid matrix, and crystalline features, i.e., the partition of the solid skeleton into individual crystals with a given distribution of orientations (crystallographic texture). Their viscoplastic behaviour is governed by the intricate interplay between these two structures [22, 23, 24]. Different studies demonstrated that the pore-to-

*Louis Védrine
Email addresses: louis.vedrine@meteo.fr (Louis Védrine), pascal.hagenmuller@meteo.fr (Pascal Hagenmuller), lionel.gelebart@cea.fr (Lionel Gélébart), maurine.montagnat@univ-grenoble-alpes.fr (Maurine Montagnat), loewe@slf.ch (Henning Löwe)

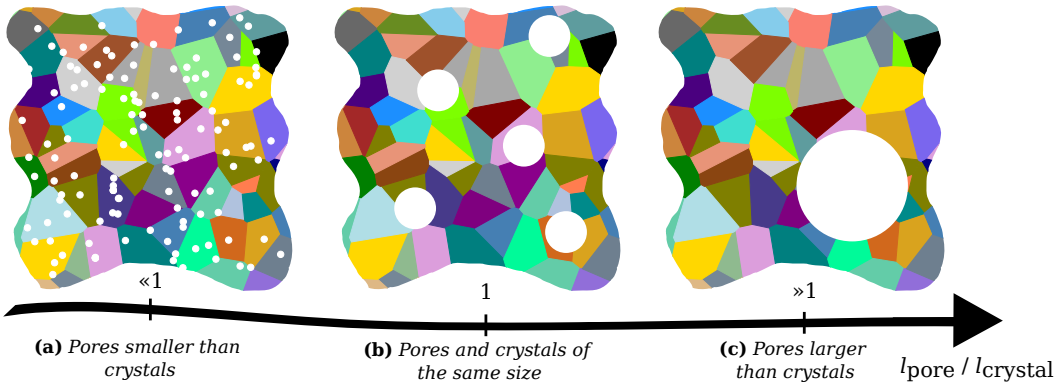

Figure 1: Exemplary microstructures of porous polycrystals with different pore-to-crystal size ratios.

crystal size ratio ($l_{\text{pore}}/l_{\text{crystal}}$) (Fig. 1), plays a critical role in the polycrystal mechanical response [e.g., 25]. Firstly, in the case of small pores inside the crystals ($l_{\text{pore}}/l_{\text{crystal}} \ll 1$, Fig. 1a), porosity mainly affects the mechanical behaviour of single crystals independently. Due to the separation of scale, a multi-scale approach is typically employed to derive the homogenised macroscopic behaviour. This process involves first determining the properties of the single crystal (typically Gurson type approach) and then deriving the overall material response (typically with FFT-based methods) [26, 27, 28, 29, 9]. Conversely, when the pore size is significantly larger than the crystal size ($l_{\text{pore}}/l_{\text{crystal}} \gg 1$, Fig. 1c), the solid matrix can be considered homogeneous due to the separation of scales [30, 31]. In this regime, the steps of the multi-scale modelling approach are inverted: first, the dense crystalline matrix is homogenised, and then the interplay between the homogeneous skeleton and the pores is derived [32]. The intermediate regime, where the pore and crystal sizes are comparable ($l_{\text{pore}}/l_{\text{crystal}} \approx 1$, Fig. 1b), presents more complex challenges and scientific results are seldom [21, 24, 33]. In this case, there is no scale separation between the pore and the crystal description so that the mechanical coupling between the two cannot generally be treated sequentially. Védrine et al. [34] demonstrated that high-porosity snow (e.g., 80% porosity) cannot be considered as a uniform dilution of pores inside crystals nor a solid matrix of homogenous ice. Lebensohn et al. [21] showed that for non-textured aggregates with low porosity in the range 0-15%, the assumption of a homogeneous matrix remains reasonable. In contrast, they also showed that for textured aggregates in the same range of porosity (especially with low strain rate sensitivity), the crystal structure must be explicitly considered. Portelette et al. [33] analysed the effect of anisotropy due to the grains surrounding the pores on the overall viscoplastic behaviour of MOX fuel (stationary creep) through crystal plasticity. They showed that, at a given porosity and crystal size, decreasing the pore size softens the material. The studies of Lebensohn et al. [21], Portelette et al. [33] focused on porosities up to 15%, which corresponds to the maximum porosity observed in nuclear fuels, such as Pu-rich agglomerates [8]. However, metal foams and snow have porosities of up to 90%. The relationship between microstructural characteristics and viscoplastic properties in highly porous polycrystals thus remains unexplored in the current literature, and previous approaches based on low and dilute porosities cannot be extrapolated [34].

This study aims to bridge the gap between the behaviour of porous and dense polycrystals across different pore-to-crystal size ratios and to understand the complex interplay between crystalline microstructure and geometrical microstructure. We use dense ice and its porous counterpart, snow, as model materials to explore how this dual microstructure influences the instantaneous viscoplastic response of porous polycrystals, assuming a constant microstructure. Indeed, dense polycrystalline ice usually serves as an ideal model for validating mechanical approaches in materials with high viscoplastic anisotropy and provides a valuable analogue for other polycrystalline materials [35, 36]. In this study, we generate synthetic microstructures to mimic the snow-ice continuum with various solid fractions and pore-to-crystal ratios. These microstructures serve as direct inputs to a 3D FFT-based solver capable of simulating the crystal plasticity at the crystal scale. These numerical experiments are used to quantify the sensitivity of the homogenised viscoplastic behaviour to the dual microstructure.

1. Material and method

1.1. Generation of synthetic microstructures

We aim to characterised the instantaneous [21, 37] viscoplastic response of polycrystalline porous material. The evolution of the microstructure under loading is not considered. Therefore, we generate synthetic microstructures by varying both the porosity and the pore-to-crystal size ratio over representative values relevant to porous polycrystals.

1.1.1. Varying the porosity

The microstructure of the dense polycrystal is generated by the Voronoi tessellation of 3375 seeds randomly distributed within a periodic volume of size 150^3 voxels (Fig. 2). Each seed results in a Voronoi cell composed of 10^3 voxels on average. Voronoï cells are simply called cells in the following.

To reduce the ice volume fraction, we follow the method described by Portelette et al. [33]: a certain number of cells are randomly selected from the initial dense polycrystal and

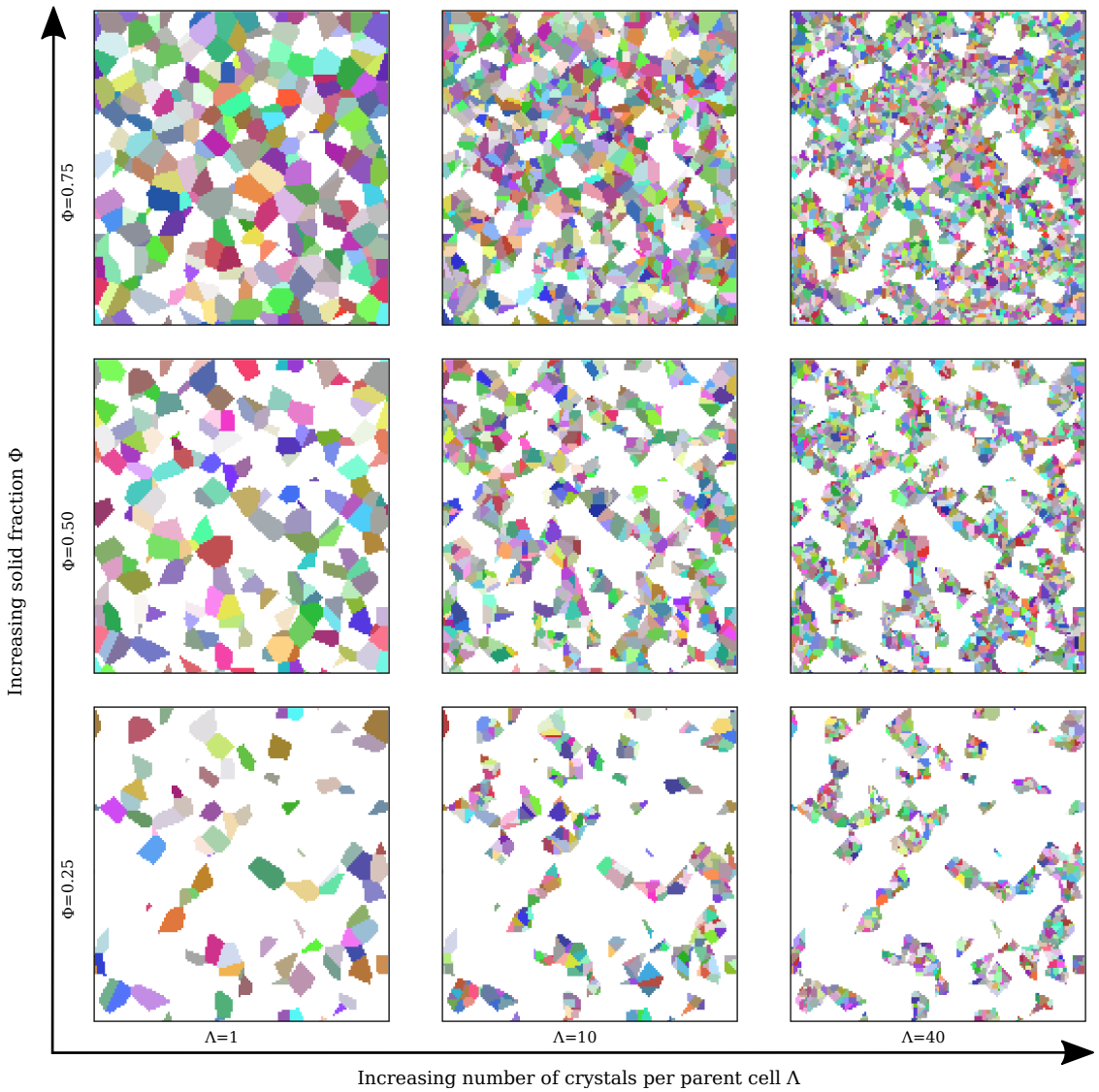

Figure 2: 2D slices of microstructures for different solid fractions Φ and numbers of crystal per Voronoi cell Λ. Pores are shown in white. Other colours are randomly assigned to individual crystals. It is important to note that the microstructure is three-dimensional, and the matrix is fully interconnected.

replaced with voids. We study a ice volume fraction between 0.25 and 1, with increments of 0.05. The minimum solid fraction is 0.25 to ensure a fully percolating structure.

1.1.2. Varying the pore-to-crystal size ratio

We aim to investigate the sensitivity of the viscoplasticity to the pore-to-crystal ratio, with all other parameters constant. Usually, the sensitivity to the pore-to-crystal ratio or porosity is explored by analysing real microstructures [38, 23] or by artificially varying the pore size [33]. However, this approach also affects the microstructure topology, which was shown to significantly influence the effective viscoplastic behaviour [37]. We explored the role of the crystalline structure at constant topology, as done by Zhao et al. [24] by subdividing each geometric cell into Λ crystals. The initial problem (Fig. 1) transforms into the problem illustrated in Figure 2.

The number of crystals per cell is randomly assigned following a Poisson distribution with a mean value of Λ crystals. We generate microstructures ranging from one crystal per cell to 40 crystals per cell. Figure 2 illustrates the diversity of microstructures generated.

We assume that the c-axis orientations of the crystals (Ice Ih has a hexagonal crystal structure, with a c/a ratio of 1.628) follow an isotropic random distribution. Only one random sample is generated for each microstructure. Indeed, Védrine et al. [34] have shown that the coefficient of variation of the simulated viscous behaviour between different samplings of the c-axis orientations remains small ($\lesssim 1.8\%$).

1.1.3. Microstructural parameters

The microstructure is characterized by its solid fraction Φ, its free surface area (SA) (air-matrix interface), and its crystal boundary surface area (CB) (Fig. 3). The solid fraction is calculated by counting the number of solid voxels in the total

volume. The interfacial surface areas are computed with the Crofton approach illustrated by Hagenmuller et al. [39].

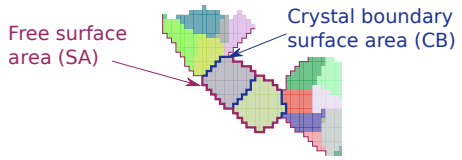

Figure 3: Definition of the interfaces.

1.2. Ice Material Properties

Isolated ice crystals deform plastically mainly through the gliding of basal dislocations [18]. Non-basal dislocations were introduced in models to accommodate basal glide in dense ice but their contribution to deformation is poorly characterized [40]. A single crystal of ice badly oriented for the glide of basal dislocations will deform at a rate at least three orders of magnitude lower than a crystal well oriented for basal glide [18].

1.2.1. Constitutive law for ice

Each crystal is modelled with a crystalline elasto-viscoplastic law. The local strain tensor $\boldsymbol{\varepsilon}^e(x)$ at position x in the solid skeleton is decomposed into the sum of an elastic and a viscoplastic part: $\boldsymbol{\varepsilon}(x) = \boldsymbol{\varepsilon}^e(x) + \boldsymbol{\varepsilon}^{vp}(x)$. The elastic strain $\boldsymbol{\varepsilon}^e(x)$ is related to the stress tensor $\boldsymbol{\sigma}(x)$ and the fourth-order stiffness tensor $\mathbf{C}(x)$ as $\boldsymbol{\sigma}(x) = \mathbf{C}(x) : \boldsymbol{\varepsilon}^e(x)$. The local elasticity tensor $\mathbf{C}(x)$ is assumed to be isotropic transverse in the crystal reference frame (C_{11} = 13.9 GPa, C_{33} = 15.0 GPa, C_{44} = 3.0 GPa, C_{12} = 7.1 GPa, C_{13} = 5.8 GPa) [41].

For the viscoplastic part, a crystal plasticity model is used, where ice crystals deform through slip on three soft basal systems, three hard prismatic systems, and six hard pyramidal systems [36]. At infinitesimal strains, the viscoplastic strain results from slips on a total of $N = 12$ different slip systems:

$$\boldsymbol{\epsilon}^{\mathrm{vp}}(x) = \sum_{k=1}^{N} \gamma^{(k)}(x)\boldsymbol{\mu}^{(k)}(x) \tag{1}$$

where $\boldsymbol{\mu}^{(k)}(x) = \boldsymbol{n}^{(k)}(x) \otimes_s \boldsymbol{b}^{(k)}(x)$ is the Schmid tensor, defined by the (symmetric) dyadic product ($\otimes_s$) of the vector normal to the glide plane $\boldsymbol{n}^{(k)}(x)$ and the Burgers vector $\boldsymbol{b}^{(k)}(x)$ of the slip system (k). The slip rate on the k-th system $\dot{\gamma}^{(k)}(x)$ is related to the resolved shear stress $\tau^{(k)}(x) = \boldsymbol{\sigma}(x) : \boldsymbol{\mu}^{(k)}(x)$ on this system by a Norton law:

$$\dot{\gamma}^{(k)}(x) = \dot{\gamma}_0^{(k)} \left(\frac{|\tau^{(k)}(x)|}{\tau_0^{(k)}} \right)^{n^{(k)}} \mathrm{sgn}(\tau^{(k)}(x)) \tag{2}$$

where $n^{(k)}$ is the stress exponent, $\dot{\gamma}_0^{(k)}$ is the reference shear rate, and $\tau_0^{(k)}$ is the critical resolved shear stress (CRSS) of slip system (k). Note that all slip systems of a given family have the same coefficients $n^{(k)}$, $\gamma_0^{(k)}$ and $\tau_0^{(k)}$.

1.2.2. Parametrization of the crystal plasticity model

Different parametrizations of the slip rates in ice have been proposed in the literature. Castelnau et al. [42], Suquet et al. [43] assumed a basal slip system exponent of 2, the value measured experimentally [44, 45, 46, 18]. Lebensohn et al. [47], Montagnat [48] assumed an exponent of 3. In practice, the exact value of the basal slip system exponent has very little impact on the viscoplasticity of dense polycrystalline ice [48]. However, this observation does not remain true for porous ice such as snow, where the basal slip system was shown to control the overall mechanical behaviour [34].

We use the parametrization from Castelnau et al. [42] and Suquet et al. [43] reported in Table 1. To the best of our knowledge, this is the most complete calibration of the ice crystal plasticity model in the literature. In particular, it correctly represents the basal slip, the dominantly active slip system. Its stress exponent, fixed at 2, agrees with experimental data on single crystals from the literature [e.g., 44, 45, 46, 18]. As we only focus on the steady-state response and to simplify comparison, the critical stresses $\tau_0^{(k)}$ are assumed to be constant with time (no hardening), and the reference shear rate is set to $\dot{\gamma}_0^{(k)} = 1\ \mathrm{s}^{-1}$. We calibrate the values of the Critical Resolved Shear Stresses (CRSS) to obtain the viscoplastic law of dense polycrystalline ice proposed by Budd and Jacka [49], Castelnau et al. [50] at -10°C (A=7.8×10^{-8} MPa^{-1} s^{-3} and $n_{poly} = 2.94$ the parameters of the Glen law for polycrystalline ice $\dot{\epsilon} = A\sigma^{n_{poly}}$). The model parameters are given in Table 1. To characterise the anisotropy of the local crystal plasticity law, we introduce two anisotropy factors $M_{b-pri} = \frac{\tau_{0,\mathrm{pri}}}{\tau_{0,\mathrm{b}}} = 5.6$ and $M_{b-pyr} = \frac{\tau_{0,\mathrm{pyr}}}{\tau_{0,\mathrm{b}}} = 3.8$. Note that additional crystal plasticity models are explored in Appendix B.1.

Table 1: Parameters of the crystal plasticity model at −10 °C [43].

Family	Systems	$n^{(k)}$	$\tau_0^{(k)}$(MPa)
Basal $[0001] < 11\bar{2}0 >$	3	2	20.6
Prismatic $[01\bar{1}0] < 2\bar{1}\bar{1}0 >$	3	2.85	114.4
Pyramidal $[11\bar{2}2] < 11\bar{2}3 >$	6	4	75.2

1.3. Simulation set-up

The simulations are performed with the Fast Fourier Transform (FFT)-based solver AMITEX_FFTP [51], using the small perturbation option. This solver employs a modified Green operator based on a hexahedral Finite Difference scheme [52] equivalent to using linear hexahedral finite elements with reduced integration [53] and an Anderson convergence acceleration technique [54], enabling the analysis of porosities (infinite contrast with the solid matrix) up to 75%. This porosity range is much larger than in previous studies such as Lebensohn et al. [21], Portelette et al. [33], which used Augmented Lagrangian schemes adapted from Michel et al. [55].

The inputs of the simulations are the 3D images of the crystal assembly and the local material law, each crystal having a single orientation within an isotropic crystallographic texture. The crystal plasticity model is implemented through the MFront code

generator [56]. The numerical integration of crystal plasticity is computationally expensive, but the solver benefits from the MPI implementation.

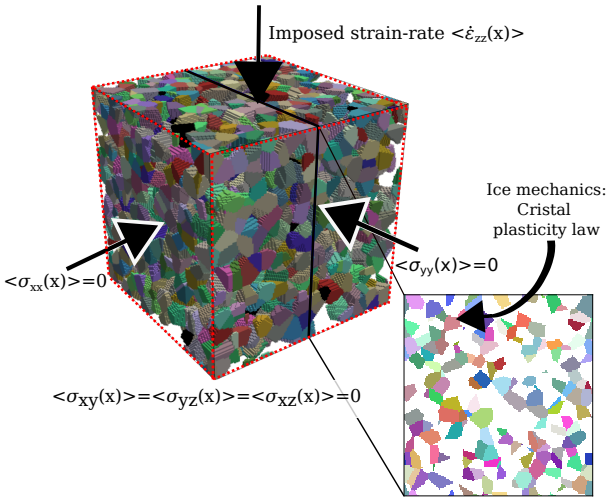

Figure 4: Numerical boundary conditions: uniaxial compression test with imposed strain rate.

Uniaxial compression tests at an imposed strain rate, $\dot{\varepsilon}_{zz}$, are performed to allow an easy comparison with experimental results reported in the literature. Using an FFT-based solver involves using periodic boundary conditions with prescribed stress or strain average components (Fig. 4). Here, we imposed the average lateral stresses ($\sigma_{xx} = \sigma_{yy} = 0$) and the average shear stresses to zero ($\sigma_{xy} = \sigma_{yz} = \sigma_{xz} = 0$), where $\varepsilon = \frac{1}{|V|}\int_V \varepsilon(x)\,\mathrm{dV} =< \varepsilon(x) >$ and $\sigma = \frac{1}{|V|}\int_V \sigma(x)\,\mathrm{dV} =< \sigma(x) >$ are respectively the volume average of the local strain and stress [57].

2. Results and discussion

The response under uniaxial compression and the identification of a homogenised model are first presented (Sect. 2.1). The sensitivity of the homogenised behaviour to the solid fraction and the crystalline structure is then quantified (Sect. 2.2 and 2.3) and gathered through a unified model (Sect. 2.4). Finally, these results are discussed in the general framework of porous polycrystals (Sect. 2.5) and in the practical case of the settlement of snow into dense ice (Sect. 2.6).

2.1. Homogenised model

Let us consider the uniaxial compression of an exemplary microstructure ($\Phi = 0.5$, $\Lambda = 1$) under strain rates ranging from $10^{-8}\,\mathrm{s}^{-1}$ to $10^{-4}\,\mathrm{s}^{-1}$. The permanent viscoplastic regime is reached after a typical strain of 0.5%. Consequently, we conduct simulations up to 1% strain to determine σ_Y (for more details see Appendix A).

To characterize the macroscopic behaviour, we aim to identify a homogenised model. Since the stress exponents of the slip systems are different (Table 1), there are no obvious reasons nor theoretical results showing that the observed behaviour should

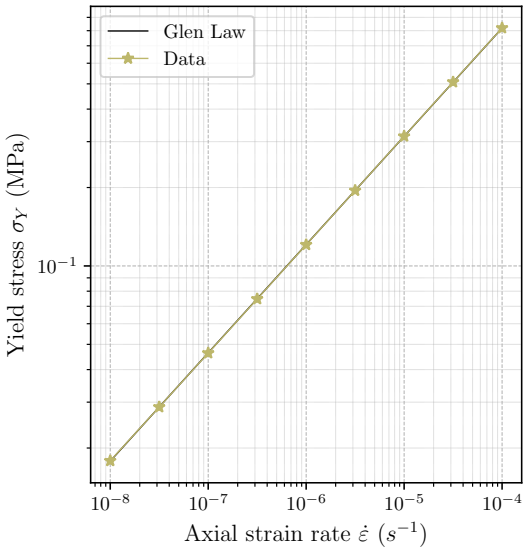

Figure 5: Axial yield stress as a function of the imposed strain rate for a given microstructure ($\Phi = 0.5$, $\Lambda = 1$) shown in Fig. 4.

be homogenisable there is no theoretical guarantee that the homogenised law can be expressed by an analytical model over a wide range of applied stresses. The evolution of the yield stress as a function of strain rate for a given microstructure ($\Phi = 0.5$, $\Lambda = 1$) is shown in Figure 5. For a given solid fraction and in the absence of hardening, the homogenized stationary behaviour relates the strain rate $\dot{\epsilon}_{zz}$ (average on the unit-cell) to the yield stress σ_{zz} (average on the unit-cell). Since, the slip systems are parametrized as power laws, a power-law relation is often a convenient form over a limited stress range to fit the numerical results:

$$\dot{\epsilon}_{zz} = \dot{\epsilon}_0 \left(\frac{\sigma_Y}{\sigma_0}\right)^n \tag{3}$$

where $\dot{\epsilon}_0$ is the prefactor set to $1\ \mathrm{s}^{-1}$ and σ_0 and n represent the macroscopic reference stress and the stress exponent, respectively. These parameters have been fitted on the simulated data ($\sigma_0 = 37.6$ MPa and $n = 2.41$ for the microstructure shown in Figure A.9). The homogenised exponent $n = 2.41$ lies between the exponents of the soft system (2.0) and those of the hard systems (2.85 and 4.0). The model perfectly reproduces the evolution of the yield stress (RMSRE=0.143%) over a broad strain rate range ($[10^{-8} - 10^{-4}]\ \mathrm{s}^{-1}$), encompassing typical ductile loading conditions (Figure 5) [58, 59]. The values of σ_0 and n are identified based on three tests conducted at imposed strain rates of $\{10^{-7}, 10^{-6}, 10^{-5}\}\ \mathrm{s}^{-1}$.

When considering slip systems with different exponents, the homogenised exponent n may depend on the stress level [13, 14]. Generally, at low stresses, the homogenised stress exponent inherits the stress exponent of the system with the lowest CRSS, and tends toward the highest stress exponent of the systems as the stress increases [60]. Consequently, the relationship between strain rate and stress no longer follows a power law. This deviation from a power law is more pronounced when the difference in exponents among the slip systems increases. Such deviations

have led to the use of more complex laws, such as the hyperbolic sine law proposed by Garofalo et al. [61] and Sellars and Tegart [62]. However, here, we observe no sensitivity to the applied stress (Fig. 5). The exponents of the slip systems in polycrystalline ice are relatively close to each other, and the anisotropy ratio (defined as the ratio of CRSS) is high [47, 63], which explains this negligible sensitivity.

2.2. *Sensitivity of the homogenised parameters to the solid fraction*

For $\Lambda = 1$, the reference stress increases with the solid fraction (Fig. 6). In other words, the presence of pores softens the material. This sensitivity is well-known [e.g., 64, 65, 66]. For large solid fractions (Φ in $[0.85, 1.0]$), an almost linear relationship between the reference stress and the solid fraction is observed, consistent with Lebensohn et al. [21], Portelette et al. [33]. However, when simulating a broader range of solid fractions (Φ in $[0.25, 1.0]$), this relationship clearly becomes non-linear.

More interestingly, the homogenised stress exponent is also found to be sensitive to the solid fraction (Fig. 6). The stress exponent is equal to that of the dense polycrystal at high solid fraction and gradually tends towards the exponent of the basal slip system when the solid fraction decreases. The sensitivity of the stress exponent to the solid fraction is related to the activity of the different slip systems. Figure 6b (background) shows the contributions of the basal, prismatic, and pyramidal slip systems to the equivalent plastic deformation p_{eq}. The basal slip system contributes the most to the plastic deformation in both dense ice (around 75% at $\Phi = 1$) and snow (99% at $\Phi = 0.25$). However, the entanglement between the slip system contributions varies with Φ. The simulations indicate that, with decreasing solid fraction, deformation accommodation between crystals is facilitated by the pore space, and does not require prismatic and pyramidal slips anymore, and the macroscopic behaviour inherits the exponent of the softest slip system. In contrast, these slips are a prerequisite for accommodating the deformation between misoriented crystals in dense ice [36]. The same experiments are conducted using different crystal plasticity laws and different exponents of soft slip systems (see Appendix B.1). In these cases, the homogenised exponent again matches that of a dense polycrystal at high solid fractions and gradually approaches the exponent of the softest slip system at low solid fractions.

These numerical results evidence the sensitivity of n to Φ, when the exponents of the soft and hard systems differ (Fig. 6). This sensitivity was already experimentally observed for metal powders during hot forming [67], as well as for snow [68]. In particular, Geindreau and Auriault [67] conducted compression tests at different strain rates and reported a sensitivity of the stress exponent to both applied stress and solid fraction. They observed that n increased from 7 to 12 with solid fractions from 0.7 to 0.95, at strain rates between 10^{-5} and 10^{-3} s^{-1}.

2.3. *Sensitivity of the homogenised parameters to the crystalline structure*

Figure 7 illustrates the evolution of the viscoplastic model as a function of solid fraction, with varying mean numbers of crystals per "geometric" cell. Interestingly, the reference stress σ_0 remains independent of the number of crystals per cell Λ. In addition, σ_0 does not depend on the choice of the exponents of the slip systems, if they yield the same dense material behaviour and are characterized by the same anisotropy ratio of the CRSS (see Appendix B.1).

In contrast, the stress exponent n varies with Λ at a given solid fraction. In terms of the stress exponent, a configuration with 20 crystals per cell and 25% solid fraction is equivalent to a microstructure where each geometric cell consists of a single crystal, but with a doubled solid fraction. At low solid fractions, we expect that the value of n will reach that of polycrystalline dense ice when the number of crystals per cell increases. However, the spatial resolution of the simulations does not enable the segmentation of one geometric cell into a very high number of crystals. Rather intuitively, when the solid fraction increases, the effect of Λ on n decreases. The viscoplastic behaviour no longer depends on Λ for dense materials ($\Phi = 1$). The assumption that one geometrical cell (one grain) equals one crystal is common in powder metallurgy and snow science [e.g., 69, 70, 71, 37]. However, several studies have observed multiple crystals per grain [72, 10, 22]. Here, we show that this assumption may strongly affect the simulated behaviour.

2.4. *A Macroscopic Viscoplastic Model*

The presented macroscopic viscoplastic model is a one-dimensional formulation derived from uniaxial compression experiments. We observe a weak sensitivity to the loading direction and to the loading type, characterised here by the stress triaxiality. This observation supports the assumption of mechanical isotropy (for more details, see Appendix B.3 and Appendix B.4).

2.4.1. *Reference stress σ_0 as a function of the solid fraction Φ*

The number of crystals per cell (Fig. 7) or the local stress exponents do not influence the reference stress (Fig. B.10). This observation suggests that σ_0 characterizes the morphology and the impact of pore distribution on stress heterogeneities rather than the local crystal-plasticity law and the crystalline structure. We can thus described σ_0 as a function of Φ only (Eq. 5). When the structure is disconnected, the reference stress is expected to be zero. To account for this percolation threshold Φ_t [73, 74] and for the portion of the solid matrix that does not support any load [75], we introduce the parameter Φ_{res}, which represents a rescaled solid fraction. This parameter is defined such that $\Phi_{res} = 0$ at the percolation threshold $\Phi = \Phi_t$ and $\Phi_{res} = 1$ at $\Phi = 1$. It can be expressed as follows:

$$\Phi_{res} = \frac{\Phi - \Phi_t}{1 - \Phi_t} \tag{4}$$

The percolation threshold depends on the type of microstructure. For our Voronoi-generated microstructure, we find that $\Phi_t = 0.2$. We fitted a power law for the reference stress as a function of Φ_{res}:

$$\sigma_0 = \sigma_{0,\Phi=1} \Phi_{res}^m. \tag{5}$$

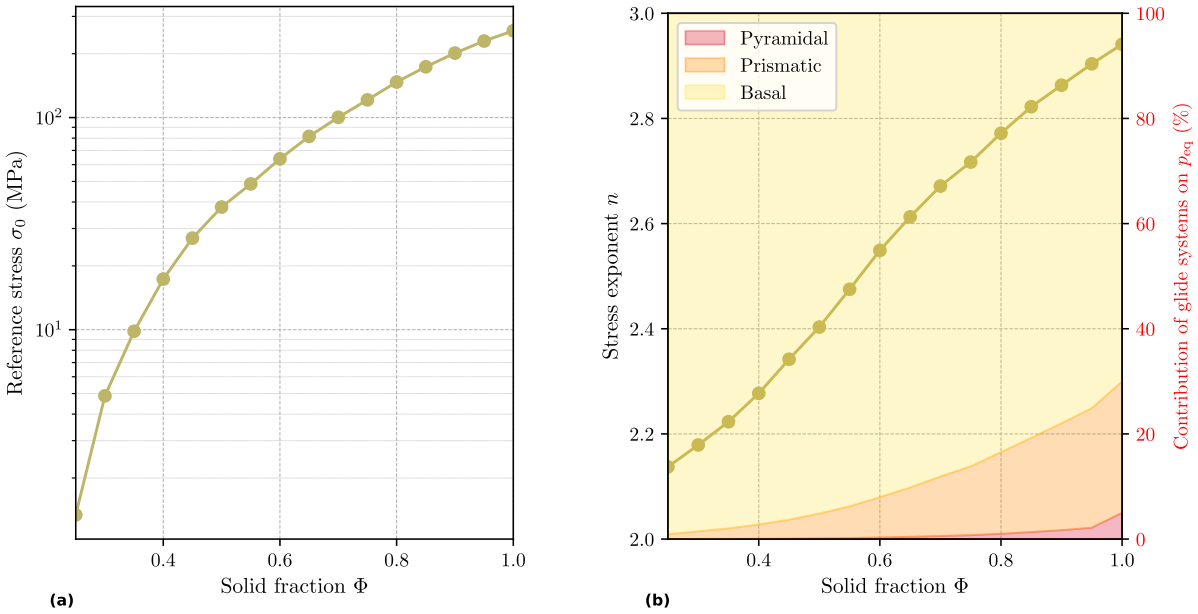

Figure 6: Parameters of the homogenised model: **(a)** reference stress σ_0 and **(b)** stress exponent n as a function of the solid fraction of a porous polycrystal. The contributions of the different glide systems to the equivalent plastic deformation p_{eq} are shown in the background of Figure b ($\Lambda = 1$).

where $\sigma_{0,\Phi=1}$ represents the reference stress of the dense polycrystal and $m = 2.02$ is the *solid fraction exponent*.

Power laws are commonly used in the literature to describe the sensitivity of mechanical properties to solid fraction, such as elastic modulus and failure strength [76, 77, 78]. In general, the parameter m characterizes the geometrical microstructure [79] and quantifies the effective structural 'backbone' of the system, which bears the majority of the load [78]. A high value of m indicates that the structure is poorly "optimized" from a mechanical perspective: the mechanical "resistance" of the microstructure will rapidly decline with increasing porosity.

Wautier et al. [32] computed the viscoplastic behaviour of snow, considering the ice matrix as homogeneous, and tested different isotropic Norton-Hoff laws for ice with an exponent between 2 and 4. They also obtained $m \approx 2$. This suggests that the type of local behaviour does not influence the parameter m. Geindreau et al. [14] obtained $m = 1.2$ for sintered metallic powders. This lower exponent indicates that the deformation heterogeneities are more pronounced in snow than in the tested metallic powder.

Remark.
- *The shape of the pores or the crystals is somehow constant in our study. However, as shown by Portelette et al. [33], pore shape plays a role in the effective behaviour. Additionally, Sevostianov and Giraud [80] demonstrated that the specific surface area of pores influences the elasticity of porous polycrystals. These factors warrant further investigation in future work.*

- *The proposed model (Eq. 5) corresponds to the one-dimensional version of the Norton-Green model [81]. The extension to three dimensions can be achieved using the formalism of the Abouaf model [82], which will be addressed in future work.*

2.4.2. *Stress exponent n as a function of frustration*

The stress exponent is sensitive to both the solid fraction and the crystalline structure (Fig. 7). The sensitivity of n to Φ is the most obvious. Indeed, Φ is the most important descriptor of porous polycrystals [83, 84]. However, when the crystalline or topological structure is changed, the solid fraction alone is not sufficient to describe the mechanical behaviour, and additional descriptors must be introduced, such as the coordination number [85, 86, 77].

In the case of viscoplastic behaviour, the stress exponent depends on the geometric frustration [87], or how easily the soft deformation mechanisms can be accommodated by the crystal surroundings (neighbours or pores) (see Sect. 2.2). The crystal frustration likely depends on the intercrystalline surface, where the basal dislocations are constrained by neighbouring crystals with different c-axes, and on the free surface (ice-air surface), where the basal dislocations are free to move. Hence, we introduce the surface area ratio r between the crystal boundaries and the free interface:

$$r = \frac{\mathrm{CB}}{\mathrm{SA}} \tag{6}$$

where CB is the intercrystalline surface area and SA is the free surface area (Fig. 3). We hereafter call r the *surface ratio*. A surface ratio of 0 indicates a high degree of freedom, while a high value indicates maximum frustration. Note that r is related to contiguity β via $\beta = r/(1 + r)$ [88].

The function $n(\Phi, r)$ has two limit cases: (i) when the crystals are fully frustrated ($[\Phi \to 1, r > 0]$ and $[\Phi > 0, r \to +\infty]$), n corresponds to the exponent of the dense polycrystal n_{poly}; (ii) when the crystals are free to deform ($[\Phi \to 0]$ and $[\Phi < 1, r \to 0]$), n corresponds to the exponent of the soft deformation mechanism n_{soft}. The contributions of these two mechanisms can be reproduced as an additional mixing rule:

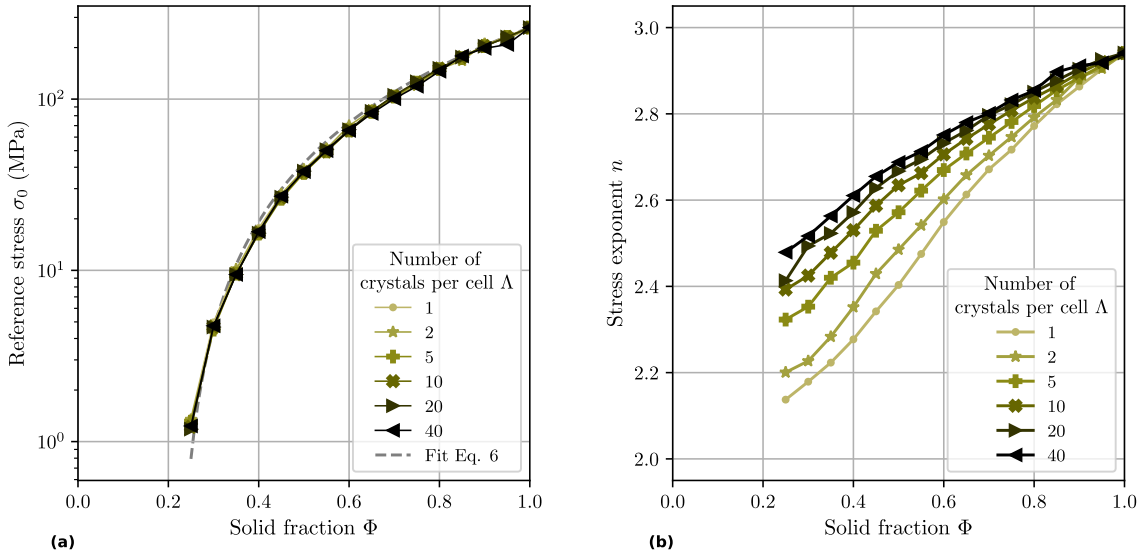

Figure 7: Parameters of the homogenised model: **(a)** reference stress σ_0 and **(b)** stress exponent n) as a function of the solid fraction Φ of a porous polycrystal for different numbers of crystals per geometric cell Λ.

$$n(\Phi, r) = n_{soft} + (n_{poly} - n_{soft})\Phi^{(r_t/r)^\gamma} \tag{7}$$

where $r_t = 1.95$ and $\gamma = 0.44$ are two fitted parameters. The model (Eq. 7) is plotted in Figure 8 and accurately reproduces the simulation data (RMSRE=1.5%). We extrapolate Eq. 7 over the entire domain of (Φ, β) in $\Omega = [0, 1] \times [0, 1]$ (Fig. 8). Our numerical experiments cover a significant portion of the domain Ω. However, certain domain areas cannot be explored with our Voronoi-generated microstructures. In particular, Φ is lower-bounded by the percolation threshold Φ_t, and low r values at high solid fractions are limited by the initial cell size. The percolation threshold inherently restricts our knowledge of the $\Phi = 0$ limit, which constitutes an abstract and unattainable bound. Different generation strategies [89, 90] or real material microstructures might help to explore the whole domain.

The surface ratio r appears to be a reliable indicator for defining the pore-to-crystal size ratios and for characterising the observed behaviour across the full pore-to-crystal ratio spectrum [e.g., 25]. Our results demonstrate that the scenarios shown in Figure 1 are governed by the stress exponent n and its sensitivity to r. When $r \gg 1$ (Fig. 1c), n corresponds to the exponent of dense polycrystals, and thus the solid matrix can be considered homogeneous, as shown by Wojtacki et al. [30], Hure [31]. Conversely, when $r \ll 1$ (Fig. 1a), n corresponds to the exponent of the soft slip system, and the material can be seen as an assembly of free sintered single crystals. Finally, the intermediate case, $r \approx 1$ (Fig. 1b), represents a smooth transition with r between the two limit cases described above (Eq. 7). In this study, the pore-to-crystal ratio is modified while maintaining a constant topology, thereby isolating the different types of mechanical behaviour. In real microstructures, however, topological changes are expected to occur, which will also affect the reference stress. Additionally, the indicator r is inherently scale-invariant, as our modelling does not introduce any characteristic length scales. Nevertheless, free surfaces likely influence dislocation mobility over a characteristic distance near the surface [91, 92, 93, 24] or geometrically necessary dislocations (GNDs) captured with gradient plasticity [94, 95] may introduce a size effect. Consequently, a scale effect homogenized law may be expected and is left for future work.

2.5. *Processes explaining the stress exponent sensitivity*

Studies showing that the stress exponent can vary with porosity are rare. Geindreau et al. [14] conducted pioneering work on this question on sintered lead powder. They fitted a hyperbolic sine viscoplastic law [61, 62] on experimental data and showed that the apparent stress exponent depends on both the stress level and the solid fraction. The sensitivity of the stress exponent to stress is well known for sinh-type creep laws [96, 97, 98, 60], but Geindreau et al. [14] also derived a dependence on the solid fraction based on the generalized Abouaf model [99]. However, we expect that the sensitivity to porosity observed by Geindreau et al. [14] was, in practice, also related to the sensitivity to stress: increasing porosity at a given applied stress increases the stress supported by the solid skeleton, which behaviour itself is sensitive to stress.

In contrast, our results reveal an intrinsic sensitivity of the stress exponent to porosity: we observe a strong sensitivity of n to Φ but no sensitivity of n to the applied stress (Section 2.1), and n depends on both Φ and r, whereas the reference stress σ_0 depends solely on Φ. Generally speaking, the stress exponent n depends on the activity of the slip systems, which can be either modulated by (i) the stress supported by the solid matrix, which is a function of the applied stress and porosity, and (ii) the frustration of the crystals, which is sensitive to porosity and intercrystalline surface area. The effect (i) is expected to dominate in the case of large differences among the local slip system exponents [14]. The effect (ii) is expected to dominate when the stress exponents are close to each other and the anisotropy ratio is large (this study). This interpretation agrees

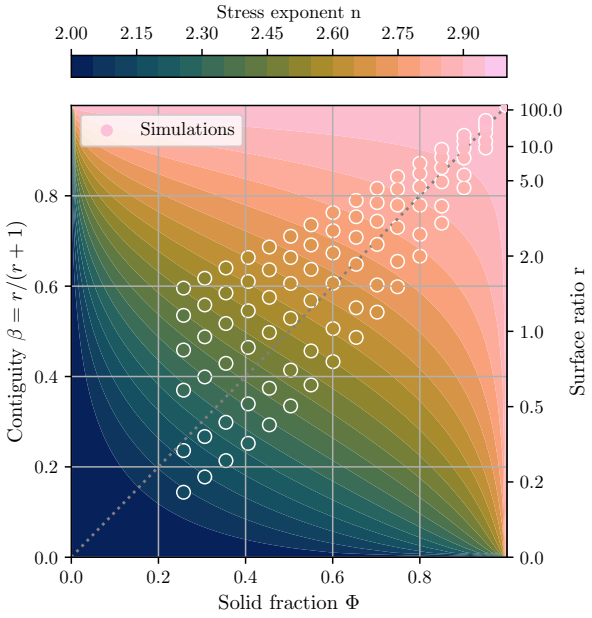

Figure 8: Stress exponent n for all the domain (Φ,β) given by the Eq. 7 background colour and simulated values based on the synthetic microstructures. The colours in the white circles correspond to the simulated stress exponents.

with previous results on dense polycrystals ($\Phi = 1$). For dense polycrystals, Bornert et al. [100] demonstrated that n decreases towards the exponent of the soft system when the anisotropy ratio M decreases. Conversely, Gilormini et al. [60] showed that n increases towards the exponent of the hard systems when the anisotropy ratio M increases. We expect that the parameters (r_t, γ) of the homogenised stress exponent (Eq. 7) depend on M. Investigating other materials, particularly those with various slip system exponents and anisotropy ratios M, would be valuable. A particularly compelling application would be the porous Zirconium (Zr–2.5Nb, $n_{\text{soft}} = 1$, $n_{\text{hard}} = 5$ and $M = \frac{\tau_{0,\text{hard}}}{\tau_{0,\text{soft}}} = 1.5$), a material utilized in pressure tubes for nuclear reactors [101] and biomedical implants [102].

2.6. *Unravelling the compaction of snow into ice*

Our results provide new insights into the mechanical compaction of snow into ice, especially in the so-called "change in the rate of densification" [e.g., 103, 104]. At the top of the snow-covered ice sheet or glacier, the ice volume fraction increases with depth in a strongly non-linear manner. Deeper down, the solid fraction increases almost linearly with depth. The transition was estimated to occur at a critical ice volume fraction of $\Phi_c = 2/3$ [105, 106]. Many authors related Φ_c to the solid fraction of a random close packing [107].

The mechanisms involved in this transition remain poorly understood. On one hand, settlement of light snow (Φ in $[0.06, 0.25]$) has been shown to follow a power viscoplastic law with an exponent close to 2 [68, 108, 109]. On the other hand, dense ice also follows a power law, called Glen's law, with an exponent close to 3, corresponding to intracrystalline deformations via dislocation creep [110]. In between, modelling attempts based on dislocation creep failed to reproduce the transition as they assumed, rather intuitively, that ice crystals in dense ice behave the same as in snow or firn (i.e., constant $n \approx 3$ with Φ) [111, 37, 32]. Therefore, the models applied to model snow-firn-ice densification were primarily empirical [112, 113, 114, 115, 104, 116]. They generally divide the densification process into two stages limited by the "critical density" [117, 118]. Alley [119] was among the first to propose a theoretical explanation for this transition in the stress exponent. He suggested a change in behaviour from grain-boundary sliding (GBS) to dislocation creep (DC) at the critical density. Indeed, a combination of GBS (with an exponent close to 1) and DC (with an exponent close to 3) enables the modelling of the low values of the measured stress exponent in snow, specifically $1.5 < n < 2.5$ [e.g., 119, 120, 121]. However, experimental evidence of GBS in field conditions remains scarce and questionable [122].

We reproduce the transition between the stress exponents of snow ($n \approx 2$) and ice ($n \approx 3$), with solely dislocation creep as the driving microscopic mechanism. Our model requires no additional mechanism, such as grain boundary sliding. The transition is solely driven by the geometrical frustration of the ice crystals, which is sensitive to ice volume fraction and intercrystalline surface area.

One may argue that our model reproduces the transition of stress exponents but does not explain why the transition should be more pronounced around the critical density $\Phi_c = 2/3$. Indeed, our model predicts a smooth transition of n with Φ at a given r without any particular feature near Φ_c (Fig. 8). We believe that the transition is not driven by the mechanical model itself but by the geometrical relationship between r and Φ that may exist in snow, firn and porous ice. We observe that for Voronoi-generated microstructures, there is a bijective relation $r(\Phi)$ for a given Λ (Fig. 8). We expect that the relation $r(\Phi)$ depends on the snow type and deviates from our synthetic microstructures. Consequently, considering solely the solid fraction is a strong assumption, highlighting the need for further investigation into the $r(\Phi)$ relationship in real microstructures.

3. Conclusion

We simulated the viscoplastic behaviour of synthetic porous polycrystals with various porosity and pore-to-crystal size ratios, thanks to full-field FFT-based simulations. Our study demonstrates that the viscoplastic behaviour of porous polycrystals can be homogenised into a power law over a broad range of stresses, even when the exponents of the different slip systems differ. While the reference stress, σ_0, depends solely on the geometric structure (i.e., the solid fraction and morphology), the stress exponent n is influenced by both the geometric and crystalline structures.

The homogenised stress exponent varies between the local stress exponents of the soft and hard deformation mechanisms and depends on their relative contribution to the total plastic

deformation. This activity is modulated by the geometric frustration of the crystals, induced by their surrounding neighbours. The range of the stress exponent has two limiting cases: (i) for low degrees of frustration (low intercrystalline surface area and low solid fraction), crystals behave as isolated single crystals, and the stress exponent corresponds to the exponent of the soft deformation mechanism; (ii) for high degrees of frustration (high intercrystalline surface area and high solid fraction), crystals are highly constrained by their neighbours, inheriting the exponents of the dense material. All in all, our study provides a physical explanation for the observed variations in stress exponents with solid fraction and stress in porous polycrystals (e.g., sintered powders Geindreau et al. [14], snow [108, 109]).

We quantify the transition between the two limiting (i) and (ii) cases with a simple model. The reference stress σ_0 is simply a power law of solid fraction. The stress exponent n can be parametrized by a mixing rule between the two limiting cases (i) and (ii) with a mixing factor depending both on solid fraction Φ and surface ratio r. This study sets a new framework for porous polycrystal viscoplasticity. In particular, the surface area ratio between the crystal boundaries and the ice-air interface appears as the relevant indicator of the pore-to-crystal size ratio. Besides this general framework, this study also paves the way for improved modelling of the snow-firn-ice continuum [123, 124].

Acknowledgements

The computations presented in this paper were performed using the GRICAD infrastructure (https://gricad.univ-grenoble-alpes.fr), which is supported by CNRS, University Grenoble Alpes and INRIA. We particularly thank Mr. Mondher CHEKKI for his help. CEN is part of LabEx OSUG@2020 (ANR-15-IDEX-02).

Author contributions: CRediT

Declaration of competing interest

The authors declare that they have no known competing financial interests or personal relationships that could have appeared to influence the work reported in this paper.

Funding

This research did not receive any specific grant from funding agencies in the public, commercial, or not-for-profit sectors.

Data availability

All materials used in this article (codes, geometric characteristic of the microstructure and numerical values, etc.) are available on Zenodo at https://zenodo.org/records/15131640?preview=1&token=eyJhbGciOiJIUzUxMiJ9.eyJpZCI6IjU0YzI4ZGU2LWU3NzgtNDhlYy05NDllLWNhMDMwMjBmNmV[illegible]YTAxY2Z[illegible]pjrxKyid74tJoqAjKiZA0HS6F34jQehoqD3Y5iW6JxybDweQVNetB4u[illegible]

Appendix A. Identification of the homogenised model

For an uniaxial compression of an exemplary microstructure ($\Phi = 0.5$, $\Lambda = 1$) under strain rates ranging from 10^{-8} s^{-1} to 10^{-4} s^{-1}, we observe three different regimes of stress evolution with strain during the compression test (Fig. A.9). First, the vertical stress σ_{zz} increases linearly with strain in an elastic regime. Then, σ_{zz} deviates from the elasticity, and the viscoplasticity is progressively activated. After this transient regime, σ_{zz} eventually reaches a constant value, the yield stress σ_Y, where the microstructure flows perfectly (stationary creep). The yield stress depends on the ice constitutive law, the microstructure and the applied strain rate. The permanent viscoplastic regime is reached after a typical strain of 0.5%. Consequently, we conduct simulations up to 1% strain to determine σ_Y.

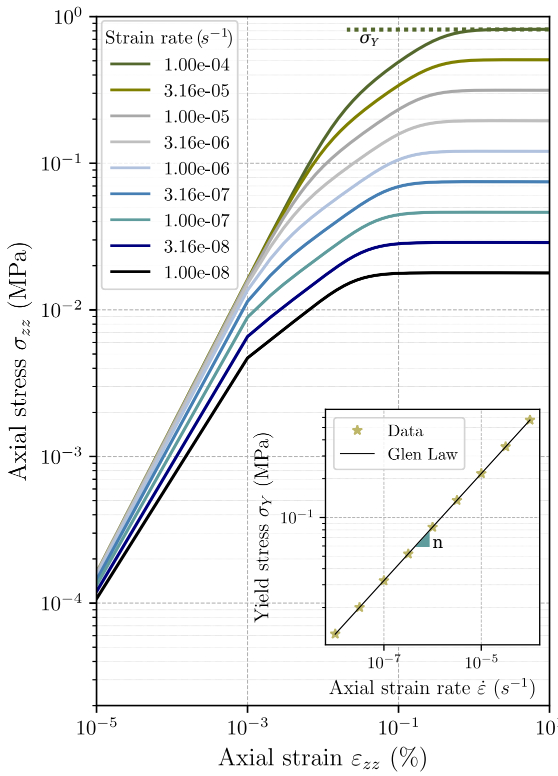

Figure A.9: Compression stress as a function of the strain for different strain rates for a given microstructure ($\Phi = 0.5$, $\Lambda = 1$) shown in Fig. 4. Inset: Axial yield strain rate as a function of the imposed strain rate .

Appendix B. Sensitivity of the homogenised model

Appendix B.1. To the ice crystal plasticity model

To study the effect of the parametrization of the crystalline plasticity law on the homogenised behaviour, we examine the effects of different crystalline plasticity laws for ice available in the literature:

- The parametrization used by Lebensohn et al. [47], where the exponents of the slip systems are set to 3, namely 3, 3, 3. This hypothesis is commonly used for dense ice, such as

Table B.2: Parameters of the crystal plasticity models at −10 °C (from of Lebensohn and Cazacu [125] and Suquet et al. [43])

Model		Our study		Lebensohn n_b=3		Lebensohn n_b=2	
Family	Systems	$n^{(k)}$	$\tau^{(k)}$(MPa)	$n^{(k)}$	$\tau^{(k)}$(MPa)	$n^{(k)}$	$\tau^{(k)}$(MPa)
Basal [0001] < $11\bar{2}0$ >	3	2	20.6	3	12.6	2	10.7
Prismatic [$01\bar{1}0$] < $2\bar{1}\bar{1}0$ >	3	2.85	114.4	3	252	3	228
Pyramidal [$11\bar{2}2$] < $11\bar{2}\bar{3}$ >	6	4	75.2	3	252	3	228

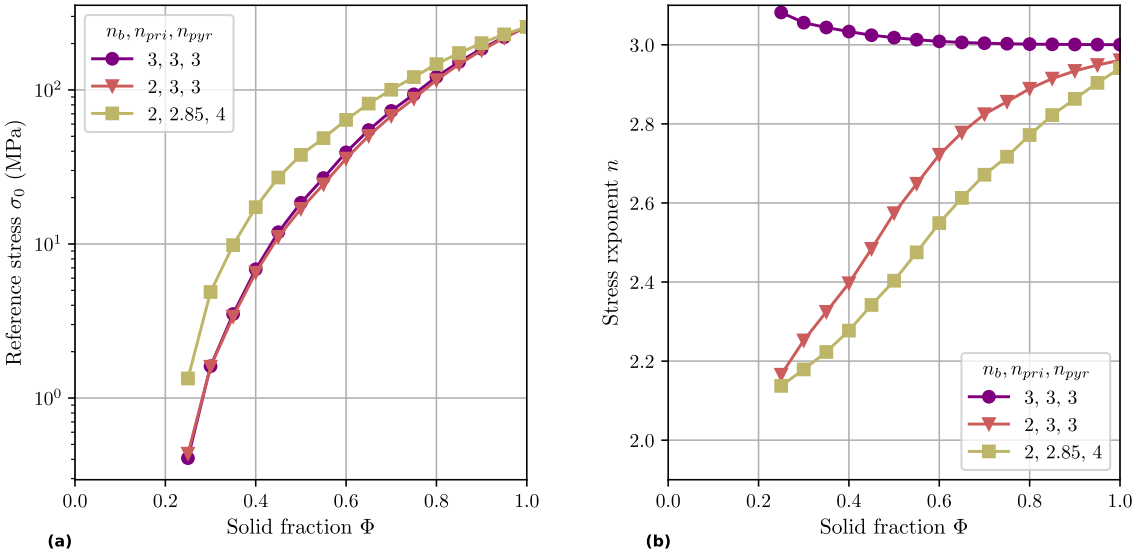

Figure B.10: Parameters of the homogenised model: **(a)** reference stress σ_0 and **(b)** stress exponent n as a function of the solid fraction of a porous polycrystal for different single-crystal ice models (Table B.2).

in studies investigating the viscoplastic development of texture [50], modelling the viscoplastic behaviour and heterogeneous intracrystalline deformation of columnar ice polycrystals [47].

- To only observe the effect of the basal slip system's stress exponent, we change only this exponent to a value of 2, to get the model name *2,3,3*. The critical resolved shear stress values are then calibrated to obtain the same response for a dense polycrystal by keeping the same anisotropy ratio $M_{b-pri} = M_{b-pyr} = 20$.

These two addition parametrisations are described in Table B.2.

Figure B.10 illustrates the evolution of the parameters of the homogenised viscoplastic law with respect to solid fraction for the two additional models. First, it is noteworthy that the sensitivity of stress to solid fraction is consistent across all three models. Interestingly, the two Lebensohn laws with the same anisotropy factor M and calibrated on a dense polycrystal yield identical curves, despite differing local exponents. This demonstrates that the reference stress depends solely on the microstructure and the anisotropy factor of the crystalline law which is lower for the Suquet law ($M_{b-pri} = 4.7$ and $M_{b-pyr} = 2.8$). Second, regardless of the chosen parametrization, the macroscopic exponent approaches that of the basal slip system.

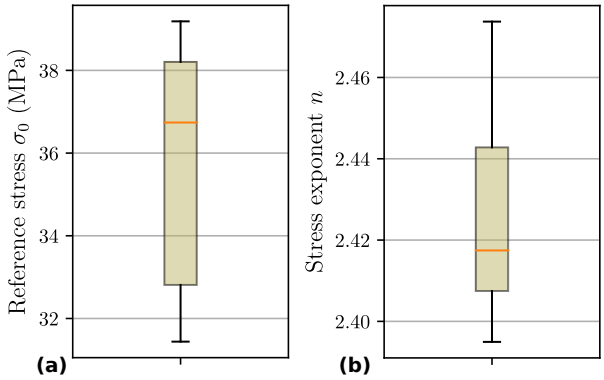

Figure B.11: ensitivity study to random draw of microstructures (10 different random samples): **(a)** Reference stress variability. **(b)** Stress exponent variability.

Appendix B.2. To the microstructure

To quantify the variability of the macroscopic response due to microstructural features (both geometrical and crystallographic), we randomly generated 10 microstructures using Voronoi tessellations, each with a solid fraction of $\phi = 0.5$ and $\lambda = 1$. The identified parameters for ten random draws of microstructures crystalline orientation are shown Figure B.11. We observe that the dispersion is small compared to the sensitivity to the solid fraction, the mean values are respectively 35.8 MPa and 2.42, the standard deviation 2.73 MPa and 0.025 for the reference stress and the stress exponent. Consequently, only a single realisation

defined by a specific geometric and crystalline configuration will be considered in this study.

Appendix B.3. To the loading direction

To assess the assumption of isotropy, uniaxial compression tests were conducted on the microstructures along the x and y directions, in addition to the z-axis, for a solid fraction of 0.25, 0.5 and 0.75. As shown in Figure B.12, the identified parameters exhibit only minor variations with loading direction, suggesting a weak influence of the sample anisotropy when compared to the sensitivity of the parameters to the solid fraction.

The relative Euclidean distance from isotropy decreases with increasing solid fraction, and the reference stress is much more sensitive to the loading direction than the stress exponent. For instance, at a solid fraction of 0.5, the directional variation is 0.2% for the stress exponent and 4.9% for the reference stress. This can be attributed to the strong dependence of the reference stress on the sample morphology, which exhibits slight geometric anisotropy—particularly at low solid fractions—since the same representative elementary volume (REV) size is retained across cases. Nevertheless, these results indicate that the size of the chosen domain (REV) is sufficient to ensure low microstructural variability with respect to the investigated loading directions. This observation supports the use of uniaxial compression tests alone to assess the sensitivity of the viscoplastic model parameters.

Appendix B.4. To the stress triaxiality

Compression tests are conducted for various triaxiality factors on a microstructure with a solid fraction of 0.25, 0.5, 0.75 and $\lambda = 1$. A vertical stress of $\sigma_z = 0.323$ MPa (corresponding to a strain rate of $10^{-7}\,\mathrm{s}^{-1}$), was imposed, while the lateral stress varied from $-\sigma_z/2$ to σ_z. In Figure B.13, the activity of the different slip systems is plotted as a function of the triaxiality factor. We observe that, for all triaxiality levels, basal slip contributes to more than 94% of the equivalent plastic strain, p_{eq}, regardless of the loading type. A very slight increase in basal activity is nevertheless observed with increasing triaxiality, with a rise of 0.3% between purely deviatoric and purely hydrostatic loading. Such an increase is minimal and comparable to that observed when increasing the solid fraction from 0.50 to 0.513. We can therefore expect the results presented to remain valid to first order under other loading conditions involving different levels of spherical stress.

References

[1] H. V. Atkinson and S. Davies. Fundamental aspects of hot isostatic pressing: An overview. *Metallurgical and Materials Transactions A*, 31(12):2981–3000, December 2000. ISSN 1543-1940. https://doi.org/10.1007/s11661-000-0078-2. URL https://doi.org/10.1007/s11661-000-0078-2.

[2] D. C. Dunand. Processing of Titanium Foams. *Advanced Engineering Materials*, 6(6):369–376, June 2004. ISSN 1438-1656, 1527-2648. https://doi.org/10.1002/adem.200405576. URL https://onlinelibrary.wiley.com/doi/10.1002/adem.200405576.

[3] M. F. Ashby. *Metal Foams: A Design Guide*. Elsevier, 2000. ISBN 978-0-7506-7219-1. Google-Books-ID: c5aKB_o2BT0C.

[4] L.-P. Lefebvre, J. Banhart, and D. C. Dunand. Porous Metals and Metallic Foams: Current Status and Recent Developments. *Advanced Engineering Materials*, 10(9):775–787, 2008. ISSN 1527-2648. https://doi.org/10.1002/adem.200800241. URL https://onlinelibrary.wiley.com/doi/abs/10.1002/adem.200800241. _eprint: https://onlinelibrary.wiley.com/doi/pdf/10.1002/adem.200800241.

[5] Rajinth Shanthar, Kun Chen, and Chamil Abeykoon. Powder-Based Additive Manufacturing: A Critical Review of Materials, Methods, Opportunities, and Challenges. *Advanced Engineering Materials*, 25(19):2300375, 2023. ISSN 1527-2648. https://doi.org/10.1002/adem.202300375. URL https://onlinelibrary.wiley.com/doi/abs/10.1002/adem.202300375. _eprint: https://onlinelibrary.wiley.com/doi/pdf/10.1002/adem.202300375.

[6] Ahmed Hassan and Ibrahim Abdullah Alnaser. A Review of Different Manufacturing Methods of Metallic Foams. *ACS Omega*, 9(6):6280–6295, February 2024. https://doi.org/10.1021/acsomega.3c08613. URL https://doi.org/10.1021/acsomega.3c08613. Publisher: American Chemical Society.

[7] Ricardo A. Lebensohn, Juan P. Escobedo, Ellen K. Cerreta, Darcie Dennis-Koller, Curt A. Bronkhorst, and John F. Bingert. Modeling void growth in polycrystalline materials. *Acta Materialia*, 61(18):6918–6932, October 2013. ISSN 1359-6454. https://doi.org/10.1016/j.actamat.2013.08.004. URL https://www.sciencedirect.com/science/article/pii/S1359645413005909.

[8] J. Noirot, L. Desgranges, and J. Lamontagne. Detailed characterisations of high burn-up structures in oxide fuels. *Journal of Nuclear Materials*, 372(2-3):318–339, January 2008. ISSN 00223115. https://doi.org/10.1016/j.jnucmat.2007.04.037. URL https://linkinghub.elsevier.com/retrieve/pii/S0022311507006666.

[9] Pierre-Guy Vincent. *Modélisation micromécanique du comportement de matériaux du nucléaire*. thesis, Université de Montpellier (UM), FRA, June 2023. URL https://irsn.hal.science/tel-04166850.

[10] Fabienne Riche, Maurine Montagnat, and Martin Schneebeli. Evolution of crystal orientation in snow during temperature gradient metamorphism. *Journal of Glaciology*, 59(213):47–55, January 2013. ISSN 0022-1430, 1727-5652. https://doi.org/10.3189/2013JoG12J116. URL https://www.cambridge.org/core/journals/journal-of-glaciology/article/evolution-of-crystal-orientation-in-snow-during-temperature-gr 9C7EDD108FBE700D4E9AE1E53DDC1E36.

[11] L. Arnaud, V. Lipenkov, J. M. Barnola, M. Gay, and P. Duval. Modelling of the densification of polar firn: characterization of the snow–firn transition. *Annals of Glaciology*, 26:39–44, January 1998. ISSN 0260-3055, 1727-5644. https://doi.org/10.3189/1998AoG26-1-39-44. URL https://www.cambridge.org/core/journals/annals-of-glaciology/article/modelling-of-the-densification-of-polar-firn-characterization-83BE4D1A995A4EDED8295E8E90A8FBD4.

[12] F. B. Swinkels, D. S. Wilkinson, E. Arzt, and M. F. Ashby. Mechanisms of hot-isostatic pressing. *Acta Metallurgica*, 31(11):1829–1840, November 1983. ISSN 0001-6160. https://doi.org/10.1016/0001-6160(83)90129-3. URL https://www.sciencedirect.com/science/article/pii/0001616083901293.

[13] J. L. Auriault, D. Bouvard, C. Dellis, and M. Lafer. Modelling of hot compaction of metal powder by homogenization. *Mechanics of Materials*, 13(3):247–255, July 1992. ISSN 0167-6636. https://doi.org/10.1016/0167-6636(92)90005-X. URL https://www.sciencedirect.com/science/article/pii/016766369290005X.

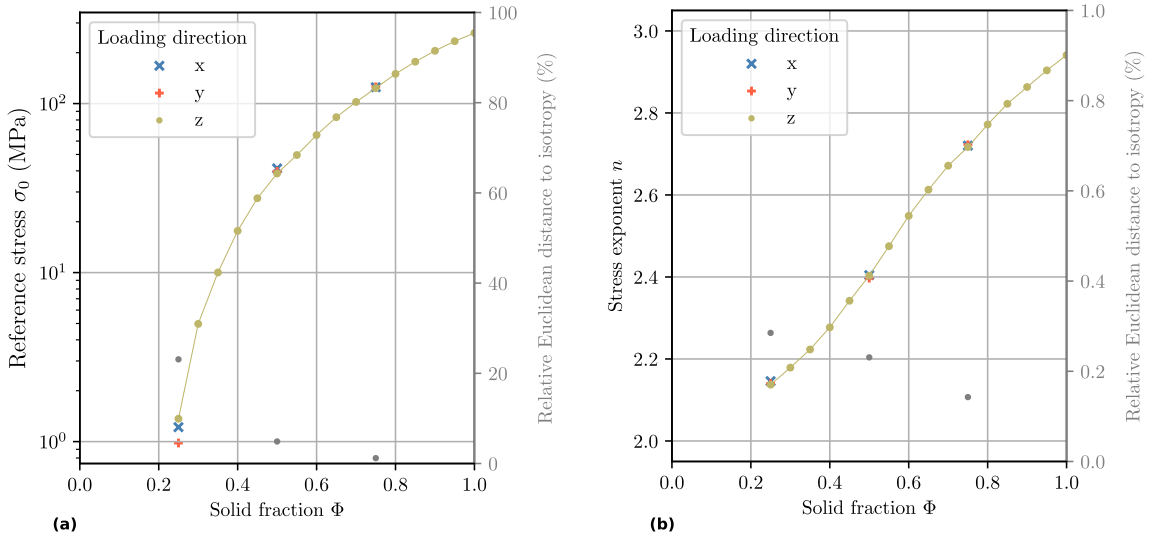

Figure B.12: Parameters of the homogenised model: **(a)** reference stress σ_0 and **(b)** stress exponent n as a function of the solid fraction of a porous polycrystal. ($\Lambda = 1$). For solid fractions of 0.25, 0.5, and 0.75, the responses to loading along the x, y, and z axes have been added, along with the relative Euclidean distance to isotropy.

[14] Christian Geindreau, Didier Bouvard, and Pierre Dorémus. Constitutive behaviour of metal powder during hot forming.: Part II: Unified viscoplastic modelling. *European Journal of Mechanics - A/Solids*, 18(4):597–615, 1999. https://doi.org/10.1016/S0997-7538(99)00101-1. URL https://hal.science/hal-00343099. Publisher: Elsevier.

[15] Charles Manière and Eugene A. Olevsky. Porosity dependence of powder compaction constitutive parameters: Determination based on spark plasma sintering tests. *Scripta Materialia*, 141:62–66, December 2017. ISSN 13596462. https://doi.org/10.1016/j.scriptamat.2017.07.026. URL https://linkinghub.elsevier.com/retrieve/pii/S1359646217304311.

[16] E. Brun, P. David, M. Sudul, and G. Brunot. A numerical model to simulate snow-cover stratigraphy for operational avalanche forecasting. *Journal of Glaciology*, 38(128):13–22, January 1992. ISSN 0022-1430, 1727-5652. https://doi.org/10.3189/S0022143000009552. URL https://www.cambridge.org/core/journals/journal-of-glaciology/article/numerical-model-to-simulate-snowcover-stratigraphy-for-operational-avalanche-forecasting/BAAC9E1F2CB6D5E01DE1C2B80A53E9DF.

[17] Michael Lehning, Perry Bartelt, Bob Brown, Charles Fierz, and Pramod Satyawali. A physical SNOWPACK model for the Swiss avalanche warning: Part II. Snow microstructure. *Cold Regions Science and Technology*, 35(3):147–167, November 2002. ISSN 0165-232X. https://doi.org/10.1016/S0165-232X(02)00073-3. URL https://www.sciencedirect.com/science/article/pii/S0165232X02000733.

[18] P. Duval, M. F. Ashby, and I. Anderman. Rate-controlling processes in the creep of polycrystalline ice. *The Journal of Physical Chemistry*, 87 (21):4066–4074, October 1983. ISSN 0022-3654, 1541-5740. https://doi.org/10.1021/j100244a014. URL https://pubs.acs.org/doi/abs/10.1021/j100244a014.

[19] R. Raj and M. F. Ashby. On grain boundary sliding and diffusional creep. *Metallurgical Transactions*, 2(4):1113–1127, April 1971. ISSN 2379-0083. https://doi.org/10.1007/BF02664244. URL https://doi.org/10.1007/BF02664244.

[20] Fabien Onimus, Thomas Jourdan, Cheng Xu, Anne A. Campbell, and Malcolm Griffiths. Irradiation creep in materials. In R. Konings and R. Stoller, editors, *Comprehensive Nuclear Materials*, volume 1, pages 310–366. Elsevier, 2021. https://doi.org/10.1016/B978-0-12-803581-8.11645-5. URL https://hal.science/hal-04065942.

[21] R.A. Lebensohn, M.I. Idiart, P. Ponte Castañeda, and P.-G. Vincent. Dilatational viscoplasticity of polycrystalline solids with intergranular cavities. *Philosophical Magazine*, 91(22):3038–3067, August 2011. ISSN 1478-6435, 1478-6443. https://doi.org/10.1080/14786435.2011.561811. URL http://www.tandfonline.com/doi/abs/10.1080/14786435.2011.561811.

[22] Jayden C. Plumb, Jonathan F. Lind, Joseph C. Tucker, Ron Kelley, and Ashley D. Spear. Three-dimensional grain mapping of open-cell metallic foam by integrating synthetic data with experimental data from high-energy X-ray diffraction microscopy. *Materials Characterization*, 144:448–460, October 2018. ISSN 1044-5803. https://doi.org/10.1016/j.matchar.2018.07.031. URL https://www.sciencedirect.com/science/article/pii/S104458031831338X.

[23] Rongxin Zhou and Han-Mei Chen. Mesoscopic investigation of size effect in notched concrete beams: The role of fracture process zone. *Engineering Fracture Mechanics*, 212:136–152, May 2019. ISSN 0013-7944. https://doi.org/10.1016/j.engfracmech.2019.03.028. URL https://www.sciencedirect.com/science/article/pii/S0013794419300025.

[24] Donglang Zhao, Kristofer E. Matheson, Brian R. Phung, Steve Petruzza, Michael W. Czabaj, and Ashley D. Spear. Investigating the effect of grain structure on compressive response of open-cell metal foam using high-fidelity crystal-plasticity modeling. *Materials Science and Engineering: A*, 812:140847, April 2021. ISSN 0921-5093. https://doi.org/10.1016/j.msea.2021.140847. URL https://www.sciencedirect.com/science/article/pii/S0921509321001167.

[25] C. Sénac, J. M. Scherer, J. Hure, T. Helfer, and B. Tanguy. Homogenized constitutive equations for porous single crystals plasticity. *European Journal of Mechanics - A/Solids*, 95:104642, September 2022. ISSN 0997-7538. https://doi.org/10.1016/j.euromechsol.2022.104642. URL https://www.sciencedirect.com/science/article/pii/S0997753822001103.

[26] Louis Joëssel, Pierre-Guy Vincent, Mihail Gărăjeu, and Martín I. Idiart. Viscoplasticity of voided cubic crystals under hydrostatic loading. *International Journal of Solids and Structures*, 147:156–165, August 2018. ISSN 0020-7683. https://doi.org/10.1016/j.ijsolstr.2018.05.022. URL https://www.sciencedirect.com/science/article/pii/S0020768318302166.

[27] Dawei Song and P. Ponte Castañeda. Macroscopic response of strongly anisotropic porous viscoplastic single crystals and applications to ice. *Extreme Mechanics Letters*, 10:41–49, January 2017. ISSN 23524316. https://doi.org/10.1016/j.eml.2016.10.001. URL https://linkinghub.elsevier.com/retrieve/pii/S2352431616301390.

[28] J. Paux, L. Morin, R. Brenner, and D. Kondo. An approximate yield criterion for porous single crystals. *European Journal of Mechanics - A/Solids*,

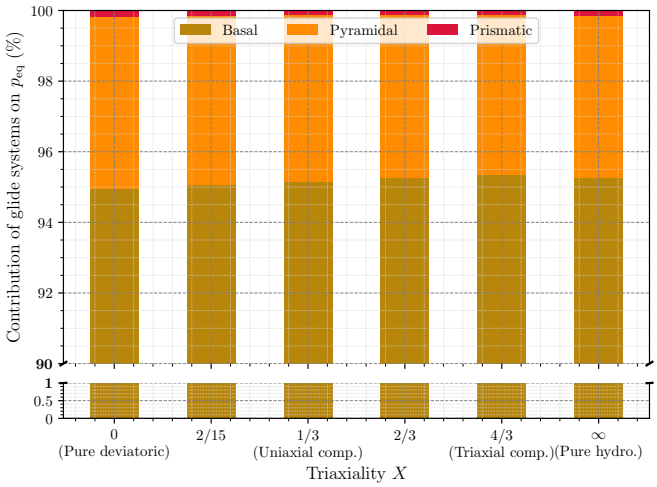

Figure B.13: Contributions of the different slip systems to the equivalent plastic strain, p_{eq}, as a function of the stress triaxiality, X.

51:1–10, May 2015. ISSN 0997-7538. https://doi.org/10.1016/j.euromechsol.2014.11.004. URL https://www.sciencedirect.com/science/article/pii/S0997753814001582.

[29] Joseph Paux, Léo Morin, and Renald Brenner. A model of porous plastic single crystals based on fractal slip lines distribution. *Journal of the Mechanics and Physics of Solids*, 167:104948, 2022. https://doi.org/10.1016/j.jmps.2022.104948. URL https://hal.science/hal-03713029. Publisher: Elsevier.

[30] Kajetan Wojtacki, Pierre-Guy Vincent, Pierre Suquet, Hervé Moulinec, and Guylaine Boittin. A micromechanical model for the secondary creep of elasto-viscoplastic porous materials with two rate-sensitivity exponents: Application to a mixed oxide fuel. *International Journal of Solids and Structures*, 184:99–113, February 2020. ISSN 00207683. https://doi.org/10.1016/j.ijsolstr.2018.12.026. URL https://linkinghub.elsevier.com/retrieve/pii/S0020768318305237.

[31] J. Hure. Yield criterion and finite strain behavior of random porous isotropic materials. *European Journal of Mechanics - A/Solids*, 85:104143, January 2021. ISSN 0997-7538. https://doi.org/10.1016/j.euromechsol.2020.104143. URL https://www.sciencedirect.com/science/article/pii/S0997753820305301.

[32] Antoine Wautier, Christian Geindreau, and Frédéric Flin. Numerical homogenization of the viscoplastic behavior of snow based on X-ray tomography images. *The Cryosphere*, 11(3):1465–1485, June 2017. ISSN 1994-0416. https://doi.org/10.5194/tc-11-1465-2017. URL https://tc.copernicus.org/articles/11/1465/2017/. Publisher: Copernicus GmbH.

[33] Luc Portelette, Pierre-Guy Vincent, Hervé Moulinec, and Mihail Gărăjeu. Viscoplastic behavior of a porous polycrystal with similar pore and grain sizes: Application to nuclear MOX fuel materials. *International Journal of Solids and Structures*, 236-237:111316, February 2022. ISSN 0020-7683. https://doi.org/10.1016/j.ijsolstr.2021.111316. URL https://www.sciencedirect.com/science/article/pii/S0020768321003954.

[34] Louis Védrine, Pascal Hagenmuller, Lionel Gélébart, Maurine Montagnat, and Antoine Bernard. Role of Ice Mechanics on Snow Viscoplasticity. *Geophysical Research Letters*, 51(7):e2023GL107676, 2024. ISSN 1944-8007. https://doi.org/10.1029/2023GL107676. URL https://onlinelibrary.wiley.com/doi/abs/10.1029/2023GL107676. _eprint: https://onlinelibrary.wiley.com/doi/pdf/10.1029/2023GL107676.

[35] D. S Wilkinson and M. F Ashby. Pressure sintering by power law creep. *Acta Metallurgica*, 23(11):1277–1285, November 1975. ISSN 0001-6160. https://doi.org/10.1016/0001-6160(75)90136-4. URL https://www.sciencedirect.com/science/article/pii/0001616075901364.

[36] Maurine Montagnat, Olivier Castelnau, P. D. Bons, S. H. Faria, O. Gagliardini, F. Gillet-Chaulet, Fanny Grennerat, A. Griera, Ricardo A. Lebensohn, and Hervé Moulinec. Multiscale modeling of ice deformation behavior. *Journal of Structural Geology*, 61:78–108, 2014. URL https://www.sciencedirect.com/science/article/pii/S0191814113000837. Publisher: Elsevier.

[37] T. Theile, H. Löwe, T. C. Theile, and M. Schneebeli. Simulating creep of snow based on microstructure and the anisotropic deformation of ice. *Acta Materialia*, 59(18):7104–7113, October 2011. ISSN 1359-6454. https://doi.org/10.1016/j.actamat.2011.07.065. URL https://www.sciencedirect.com/science/article/pii/S1359645411005519.

[38] Kyu-Sik Kim, Jung-Yeol Yun, Baig-Gyu Choi, and Kee-Ahn Lee. Effect of the pore size on the creep deformation behavior of Ni-Fe-Cr-Al porous metal. *Metals and Materials International*, 20(3):507–513, May 2014. ISSN 1598-9623, 2005-4149. https://doi.org/10.1007/s12540-014-3015-4. URL http://link.springer.com/10.1007/s12540-014-3015-4.

[39] Pascal Hagenmuller, Margret Matzl, Guillaume Chambon, and Martin Schneebeli. Sensitivity of snow density and specific surface area measured by microtomography to different image processing algorithms. *The Cryosphere*, 10(3):1039–1054, May 2016. ISSN 1994-0416. https://doi.org/10.5194/tc-10-1039-2016. URL https://tc.copernicus.org/articles/10/1039/2016/. Publisher: Copernicus GmbH.

[40] Takeo Hondoh. Nature and behavior of dislocations in ice. In *Physics of ice core records*, pages 3–24. Hokkaido University Press, 2000.

[41] P. H. Gammon, H. Kiefte, M. J. Clouter, and W. W. Denner. Elastic Constants of Artificial and Natural Ice Samples by Brillouin Spectroscopy. *Journal of Glaciology*, 29(103):433–460, January 1983. ISSN 0022-1430, 1727-5652. https://doi.org/10.3189/S0022143000030355. URL https://www.cambridge.org/core/journals/journal-of-glaciology/article/elastic-constants-of-artificial-and-natural-ice-samples-by-bri 0C027E622189AE838C8FC631371BD94C.

[42] O. Castelnau, P. Duval, M. Montagnat, and R. Brenner. Elastoviscoplastic micromechanical modeling of the transient creep of ice. *Journal of Geophysical Research: Solid Earth*, 113(B11), 2008. ISSN 2156-2202. https://doi.org/10.1029/2008JB005751. URL https://onlinelibrary.wiley.com/doi/abs/10.1029/2008JB005751. _eprint: https://onlinelibrary.wiley.com/doi/pdf/10.1029/2008JB005751.

[43] P. Suquet, H. Moulinec, O. Castelnau, M. Montagnat, N. Lahellec, F. Grennerat, P. Duval, and R. Brenner. Multi-scale modeling of the mechanical behavior of polycrystalline ice under transient creep. *Procedia IUTAM*, 3:76–90, 2012. ISSN 22109838. https://doi.org/10.1016/j.piutam.2012.03.006. URL https://linkinghub.

elsevier.com/retrieve/pii/S2210983812000077.

[44] D. T. Griggs and N. E. Coles. *Creep of Single Crystals of Ice*. U.S. Army Snow Ice and Permafrost Research Establishment, Corps of Engineers, 1954. Google-Books-ID: 6rj90QfwRpQC.

[45] R. O. Ramseier. *Growth and mechanical properties of river and lake ice*. PhD Thesis, éditeur non identifié, 1975.

[46] D. R. Homer and J. W. Glen. The Creep Activation Energies of Ice. *Journal of Glaciology*, 21(85):429–444, January 1978. ISSN 0022-1430, 1727-5652. https://doi.org/10.3189/S0022143000033591. URL https://www.cambridge.org/core/journals/journal-of-glaciology/article/creep-activation-energies-of-ice/F3C450FC12EE14D50B75546071B7CB31.

[47] R.A. Lebensohn, M. Montagnat, P. Mansuy, P. Duval, J. Meysonnier, and A. Philip. Modeling viscoplastic behavior and heterogeneous intracrystalline deformation of columnar ice polycrystals. *Acta Materialia*, 57 (5):1405–1415, March 2009. ISSN 13596454. https://doi.org/10.1016/j.actamat.2008.10.057. URL https://linkinghub.elsevier.com/retrieve/pii/S1359645408008318.

[48] Maurine Montagnat. *Contribution à l'étude du comportement viscoplastique des glaces des calottes polaires : modes de déformation et simulation du développement des textures*. phdthesis, Université Joseph-Fourier - Grenoble I, November 2001. URL https://theses.hal.science/tel-00010695.

[49] W. F. Budd and T. H. Jacka. A review of ice rheology for ice sheet modelling. *Cold Regions Science and Technology*, 16(2):107–144, July 1989. ISSN 0165-232X. https://doi.org/10.1016/0165-232X(89)90014-1. URL https://www.sciencedirect.com/science/article/pii/0165232X89900141.

[50] Olivier Castelnau, Paul Duval, Ricardo A. Lebensohn, and Gilles R. Canova. Viscoplastic modeling of texture development in polycrystalline ice with a self-consistent approach: Comparison with bound estimates. *Journal of Geophysical Research: Solid Earth*, 101(B6): 13851–13868, 1996. https://doi.org/https://doi.org/10.1029/96JB00412. URL https://agupubs.onlinelibrary.wiley.com/doi/abs/10.1029/96JB00412. _eprint: https://agupubs.onlinelibrary.wiley.com/doi/pdf/10.1029/96JB00412.

[51] L. Gelebart, J. Derouillat, N. Doucet, F. Ouaki, A. Marano, and J. Duverge. Amitex_fftp, 2020.

[52] François Willot. Fourier-based schemes for computing the mechanical response of composites with accurate local fields. *Comptes Rendus Mécanique*, 343(3):232–245, March 2015. ISSN 16310721. https://doi.org/10.1016/j.crme.2014.12.005. URL https://linkinghub.elsevier.com/retrieve/pii/S1631072114002149.

[53] Matti Schneider, Dennis Merkert, and Matthias Kabel. FFT-based homogenization for microstructures discretized by linear hexahedral elements. *International Journal for Numerical Methods in Engineering*, 109(10):1461–1489, 2017. ISSN 1097-0207. https://doi.org/10.1002/nme.5336. URL https://onlinelibrary.wiley.com/doi/abs/10.1002/nme.5336. _eprint: https://onlinelibrary.wiley.com/doi/pdf/10.1002/nme.5336.

[54] Donald G. Anderson. Iterative Procedures for Nonlinear Integral Equations. *Journal of the ACM*, 12(4):547–560, October 1965. ISSN 0004-5411, 1557-735X. https://doi.org/10.1145/321296.321305. URL https://dl.acm.org/doi/10.1145/321296.321305.

[55] J. C. Michel, H. Moulinec, and P. Suquet. A computational scheme for linear and non-linear composites with arbitrary phase contrast. *International Journal for Numerical Methods in Engineering*, 52(1-2):139–160, 2001. ISSN 1097-0207. https://doi.org/10.1002/nme.275. URL https://onlinelibrary.wiley.com/doi/abs/10.1002/nme.275. _eprint: https://onlinelibrary.wiley.com/doi/pdf/10.1002/nme.275.

[56] Thomas Helfer, Bruno Michel, Jean-Michel Proix, Maxime Salvo, Jérôme Sercombe, and Michel Casella. Introducing the open-source mfront code generator: Application to mechanical behaviours and material knowledge management within the PLEIADES fuel element modelling platform. *Computers & Mathematics with Applications*, 70(5):994–1023, September 2015. ISSN 0898-1221. https://doi.org/10.1016/j.camwa.2015.06.027. URL https://www.sciencedirect.com/science/article/pii/S0898122115003132.

[57] R. Hill. Elastic properties of reinforced solids: Some theoretical principles. *Journal of the Mechanics and Physics of Solids*, 11(5):357–372, September 1963. ISSN 0022-5096. https://doi.org/10.1016/0022-5096(63)90036-X. URL https://www.sciencedirect.com/science/article/pii/002250966390036X.

[58] Hidek Narita. Mechanical behaviour and structure of snow under uniaxial tensile stress. *Journal of Glaciology*, 26(94):275–282, 1980. ISSN 0022-1430, 1727-5652. https://doi.org/10.3189/S0022143000010819. URL https://www.cambridge.org/core/product/identifier/S0022143000010819/type/journal_article.

[59] Antoine Bernard. *Etude multiéchelle de la transition ductile-fragile dans la neige*. phdthesis, Université Grenoble Alpes [2020-....], March 2023. URL https://theses.hal.science/tel-04145610.

[60] P. Gilormini, M. V. Nebozhyn, and P. Ponte Castañeda. Accurate estimates for the creep behavior of hexagonal polycrystals. *Acta Materialia*, 49(2):329–337, January 2001. ISSN 1359-6454. https://doi.org/10.1016/S1359-6454(00)00319-0. URL https://www.sciencedirect.com/science/article/pii/S1359645400003190.

[61] F. Garofalo, O. Richmond, W. F. Domis, and F. von Gemmingen. Paper 30: Strain-Time, Rate-Stress and Rate-Temperature Relations during Large Deformations in Creep. *Proceedings of the Institution of Mechanical Engineers, Conference Proceedings*, 178(1):1–31, June 1963. ISSN 0367-8849. https://doi.org/10.1243/PIME_CONF_1963_178_010_02. URL https://doi.org/10.1243/PIME_CONF_1963_178_010_02. Num Pages: 1-39 Publisher: IMECHE.

[62] C. M. Sellars and W. J. McG. Tegart. Hot Workability. *International Metallurgical Reviews*, 17(1):1–24, January 1972. ISSN 0367-9020. https://doi.org/10.1179/imtlr.1972.17.1.1. URL https://journals.sagepub.com/doi/abs/10.1179/imtlr.1972.17.1.1. Publisher: SAGE Publications.

[63] M. Montagnat, N. Azuma, D. Dahl-Jensen, J. Eichler, S. Fujita, F. Gillet-Chaulet, S. Kipfstuhl, D. Samyn, A. Svensson, and I. Weikusat. Fabric along the NEEM ice core, Greenland, and its comparison with GRIP and NGRIP ice cores. *The Cryosphere*, 8(4):1129–1138, July 2014. ISSN 1994-0416. https://doi.org/10.5194/tc-8-1129-2014. URL https://tc.copernicus.org/articles/8/1129/2014/. Publisher: Copernicus GmbH.

[64] M. F. Ashby and P. Duval. The creep of polycrystalline ice. *Cold Regions Science and Technology*, 11(3):285–300, November 1985. ISSN 0165-232X. https://doi.org/10.1016/0165-232X(85)90052-7. URL https://www.sciencedirect.com/science/article/pii/0165232X85900527.

[65] A. C. F. Cocks. Inelastic deformation of porous materials. *Journal of the Mechanics and Physics of Solids*, 37(6):693–715, January 1989. ISSN 0022-5096. https://doi.org/10.1016/0022-5096(89)90014-8. URL https://www.sciencedirect.com/science/article/pii/0022509689900148.

[66] J. M. Duva and P. D. Crow. The densification of powders by power-law creep during hot isostatic pressing. *Acta Metallurgica et Materialia*, 40(1): 31–35, January 1992. ISSN 0956-7151. https://doi.org/10.1016/0956-7151(92)90196-L. URL https://www.sciencedirect.com/science/article/pii/095671519290196L.

[67] Christian Geindreau and Jean-Louis Auriault. Investigation of the viscoplastic behaviour of alloys in the semi-solid state by homogenization. *Mechanics of Materials*, 31(8):535–551, 1999. https://doi.org/10.1016/S0167-6636(99)00012-5. URL https://hal.science/hal-00343101. Publisher: Elsevier.

[68] Carlo Scapozza and Perry A. Bartelt. The influence of temperature on the small-strain viscous deformation mechanics of snow: a comparison with polycrystalline ice. *Annals of Glaciology*, 37:90–96, January 2003. ISSN 0260-3055, 1727-5644. https://doi.org/10.3189/172756403781815410. URL https://www.cambridge.org/core/journals/annals-of-glaciology/article/influence-of-temperature-on-the-smallstrain-viscous-deformatio 15AC18BC2158259E1B53416DE1FCF645.

[69] E. Arzt, M. F. Ashby, and K. E. Easterling. Practical applications of hotisostatic Pressing diagrams: Four case studies. *Metallurgical Transactions A*, 14(1):211–221, February 1983. ISSN 2379-0180. https://doi.org/10.1007/BF02651618. URL https://

doi.org/10.1007/BF02651618.

[70] P. R. Kry. Quantitative Stereological Analysis of Grain Bonds in Snow. *Journal of Glaciology*, 14(72):467–477, January 1975. ISSN 0022-1430, 1727-5652. https://doi.org/10.3189/S0022143000021973. URL https://www.cambridge.org/core/journals/journal-of-glaciology/article/quantitative-stereological-analysis-of-grain-bonds-in-snow/3AAEBFFB8EF87B9DA152F26D616ECBD4.

[71] J. Freitag, S. Kipfstuhl, and S. H. Faria. The connectivity of crystallite agglomerates in low-density firn at Kohnen station, Dronning Maud Land, Antarctica. *Annals of Glaciology*, 49:114–120, January 2008. ISSN 0260-3055, 1727-5644. https://doi.org/10.3189/172756408787814852. URL https://www.cambridge.org/core/journals/annals-of-glaciology/article/connectivity-of-crystallite-agglomerates-in-lowdensity-firn-at-kohnen-station-dronning-maud-land-antarctica/101911ADC0AC3C4331AD2BEC3636169C.

[72] J. Zhou, S. Allameh, and W. O. Soboyejo. Microscale testing of the strut in open cell aluminum foams. *Journal of Materials Science*, 40(2):429–439, January 2005. ISSN 1573-4803. https://doi.org/10.1007/s10853-005-6100-8. URL https://doi.org/10.1007/s10853-005-6100-8.

[73] D. J. Green. An introduction to the mechanical properties of ceramics, 1998.

[74] Dietrich Stauffer and Ammon Aharony. *Introduction To Percolation Theory: Second Edition*. Taylor & Francis, London, 2 edition, December 2018. ISBN 978-1-315-27438-6. https://doi.org/10.1201/9781315274386.

[75] L. E. Holman and H. Leuenberger. The relationship between solid fraction and mechanical properties of compacts — the percolation theory model approach. *International Journal of Pharmaceutics*, 46(1):35–44, September 1988. ISSN 0378-5173. https://doi.org/10.1016/0378-5173(88)90007-5. URL https://www.sciencedirect.com/science/article/pii/0378517388900075.

[76] A. Wautier, C. Geindreau, and F. Flin. Linking snow microstructure to its macroscopic elastic stiffness tensor: A numerical homogenization method and its application to 3-D images from X-ray tomography. *Geophysical Research Letters*, 42(19):8031–8041, 2015. ISSN 1944-8007. https://doi.org/10.1002/2015GL065227. URL https://onlinelibrary.wiley.com/doi/abs/10.1002/2015GL065227. _eprint: https://onlinelibrary.wiley.com/doi/pdf/10.1002/2015GL065227.

[77] Johan Gaume, Henning Löwe, Shurun Tan, and Leung Tsang. Scaling laws for the mechanics of loose and cohesive granular materials based on Baxter's sticky hard spheres. *Physical Review E*, 96(3):032914, September 2017. https://doi.org/10.1103/PhysRevE.96.032914. URL https://link.aps.org/doi/10.1103/PhysRevE.96.032914. Publisher: American Physical Society.

[78] Lars Blatny, Henning Löwe, Stephanie Wang, and Johan Gaume. Computational micromechanics of porous brittle solids. *Computers and Geotechnics*, 140:104284, December 2021. ISSN 0266-352X. https://doi.org/10.1016/j.compgeo.2021.104284. URL https://www.sciencedirect.com/science/article/pii/S0266352X21002822.

[79] Giovanni Bruno, Alexander M. Efremov, Andreyi N. Levandovskyi, and Bjorn Clausen. Connecting the macro- and microstrain responses in technical porous ceramics: modeling and experimental validations. *Journal of Materials Science*, 46(1):161–173, January 2011. ISSN 1573-4803. https://doi.org/10.1007/s10853-010-4899-0. URL https://doi.org/10.1007/s10853-010-4899-0.

[80] Igor Sevostianov and Albert Giraud. On the Compliance Contribution Tensor for a Concave Superspherical Pore. *International Journal of Fracture*, 177(2):199–206, October 2012. ISSN 1573-2673. https://doi.org/10.1007/s10704-012-9754-7. URL https://doi.org/10.1007/s10704-012-9754-7.

[81] R. J. Green. A plasticity theory for porous solids. *International Journal of Mechanical Sciences*, 14(4):215–224, April 1972. ISSN 0020-7403. https://doi.org/10.1016/0020-7403(72)90063-X. URL https://www.sciencedirect.com/science/article/pii/002074037290063X.

[82] Marc Abouaf. *Modélisation de la compaction de poudres métalliques frittées : approche par la mécanique des milieux continus*. 1985. Pages: 186 p.

[83] Andreas Fritsch, Christian Hellmich, and Philippe Young. Micromechanics-Derived Scaling Relations for Poroelasticity and Strength of Brittle Porous Polycrystals. *Journal of Applied Mechanics*, 80(020905), February 2013. ISSN 0021-8936. https://doi.org/10.1115/1.4007922. URL https://doi.org/10.1115/1.4007922.

[84] Claire Morin, Viktoria Vass, and Christian Hellmich. Micromechanics of elastoplastic porous polycrystals: Theory, algorithm, and application to osteonal bone. *International Journal of Plasticity*, 91:238–267, April 2017. ISSN 07496419. https://doi.org/10.1016/j.ijplas.2017.01.009. URL https://linkinghub.elsevier.com/retrieve/pii/S0749641917300517.

[85] H. Riedel, H. Zipse, and J. Svoboda. Equilibrium pore surfaces, sintering stresses and constitutive equations for the intermediate and late stages of sintering—II. Diffusional densification and creep. *Acta Metallurgica et Materialia*, 42(2):445–452, February 1994. ISSN 0956-7151. https://doi.org/10.1016/0956-7151(94)90499-5. URL https://www.sciencedirect.com/science/article/pii/0956715194904995.

[86] Ran Liu and Antonia Antoniou. A relationship between the geometrical structure of a nanoporous metal foam and its modulus. *Acta Materialia*, 61(7):2390–2402, April 2013. ISSN 1359-6454. https://doi.org/10.1016/j.actamat.2013.01.011. URL https://www.sciencedirect.com/science/article/pii/S1359645413000232.

[87] Roderich Moessner and Arthur P. Ramirez. Geometrical frustration. *Physics Today*, 59(2):24–29, February 2006. ISSN 0031-9228. https://doi.org/10.1063/1.2186278. URL https://doi.org/10.1063/1.2186278.

[88] Ervin E. Underwood. *Quantitative Stereology*. Addison-Wesley, Reading, Mass.,, 1970.

[89] Romain Quey and Matthew Kasemer. The Neper/FEPX Project: Free / Open-source Polycrystal Generation, Deformation Simulation, and Post-processing. *IOP Conference Series: Materials Science and Engineering*, 1249(1):012021, July 2022. ISSN 1757-899X. https://doi.org/10.1088/1757-899X/1249/1/012021. URL https://dx.doi.org/10.1088/1757-899X/1249/1/012021. Publisher: IOP Publishing.

[90] Lars Blatny, Henning Löwe, and Johan Gaume. *GRFsaw: A lightweight stochastic microstructure generator*. December 2024. https://doi.org/10.48550/arXiv.2412.05168.

[91] Virginie Goussery, Yves Bienvenu, Samuel Forest, Anne-Françoise Gourgues, Christophe Colin, and Jean-Dominique Bartout. Grain size effects on the mechanical behavior of open-cell nickel foams. *Advanced Engineering Materials*, 6:432–439, 2004. https://doi.org/10.1002/adem.200405153. URL https://hal.science/hal-00165963. Publisher: Wiley-VCH Verlag.

[92] Chin-Long Lee and Shaofan Li. A half-space Peierls–Nabarro model and the mobility of screw dislocations in a thin film. *Acta Materialia*, 55(6):2149–2157, April 2007. ISSN 1359-6454. https://doi.org/10.1016/j.actamat.2006.11.015. URL https://www.sciencedirect.com/science/article/pii/S1359645406008263.

[93] Joshua C. Crone, Lynn B. Munday, and Jaroslaw Knap. Capturing the effects of free surfaces on void strengthening with dislocation dynamics. *Acta Materialia*, 101:40–47, December 2015. ISSN 1359-6454. https://doi.org/10.1016/j.actamat.2015.08.067. URL https://www.sciencedirect.com/science/article/pii/S1359645415006540.

[94] Samuel Forest, Rainer Sievert, and Elias C. Aifantis. Strain Gradient Crystal Plasticity: Thermomechanical Formulations and Applications. *Journal of the Mechanical Behavior of Materials*, 13(3-4):219–232, August 2002. ISSN 2191-0243. https://doi.org/10.1515/JMBM.2002.13.3-4.219. URL https://www.degruyterbrill.com/document/doi/10.1515/JMBM.2002.13.3-4.219/html. Publisher: De Gruyter.

[95] K. L. Nielsen and C. F. Niordson. A numerical basis for strain-gradient plasticity theory: Rate-independent and rate-dependent formulations. *Journal of the Mechanics and Physics of Solids*, 63:113–127, February 2014. ISSN 0022-5096. https://doi.org/10.1016/j.jmps.2013.09.018. URL https://www.sciencedirect.com/science/article/pii/S0022509613002019.

[96] Johannes Weertman. Creep deformation of ice. *Annual Review of Earth and Planetary Sciences, Vol. 11, p. 215*, 11:215, 1983. URL https://adsabs.harvard.edu/full/1983AREPS..11..215W.

[97] Yong-Mei Liu, H. N. G. Wadley, and J. M. Duva. Densification of porous materials by power-law creep. *Acta Metallurgica et Materialia*, 42(7):2247–2260, July 1994. ISSN 0956-7151. https://doi.org/10.1016/0956-7151(94)90303-4. URL https://www.sciencedirect.com/science/article/pii/0956715194903034.

[98] R. E. Dutton, S. L. Semiatin, and R. L. Goetz. Validation of computer models for the consolidation of metal—matrix composites. *Materials Science and Engineering: A*, 221(1):85–93, December 1996. ISSN 0921-5093. https://doi.org/10.1016/S0921-5093(96)10456-1. URL https://www.sciencedirect.com/science/article/pii/S0921509396104561.

[99] M. Abouaf, J. L. Chenot, G. Raisson, and P. Bauduin. Finite element simulation of hot isostatic pressing of metal powders. *International Journal for Numerical Methods in Engineering*, 25(1):191–212, 1988. ISSN 1097-0207. https://doi.org/10.1002/nme.1620250116. URL https://onlinelibrary.wiley.com/doi/abs/10.1002/nme.1620250116. _eprint: https://onlinelibrary.wiley.com/doi/pdf/10.1002/nme.1620250116.

[100] M. Bornert, R. Masson, P. Ponte Castañeda, and A. Zaoui. Second-order estimates for the effective behaviour of viscoplastic polycrystalline materials. *Journal of the Mechanics and Physics of Solids*, 49(11):2737–2764, November 2001. ISSN 0022-5096. https://doi.org/10.1016/S0022-5096(01)00077-1. URL https://www.sciencedirect.com/science/article/pii/S0022509601000771.

[101] N. Christodoulou and C. N. Tomé. Anisotropy of plastic flow in Zr-2.5Nb pressure tube material analysed using a viscoplastic self-consistent approach. *Acta Materialia*, 283:120503, January 2025. ISSN 1359-6454. https://doi.org/10.1016/j.actamat.2024.120503. URL https://www.sciencedirect.com/science/article/pii/S1359645424008528.

[102] A. E. Aguilar Maya, D. R. Grana, A. Hazarabedian, G. A. Kokubu, M. I. Luppo, and G. Vigna. Zr–Ti–Nb porous alloys for biomedical application. *Materials Science and Engineering: C*, 32(2):321–329, March 2012. ISSN 0928-4931. https://doi.org/10.1016/j.msec.2011.10.035. URL https://www.sciencedirect.com/science/article/pii/S0928493111003079.

[103] Joseph K. Landauer. Some Preliminary Observations on the Plasticity of Greenland Glaciers. *Journal of Glaciology*, 3(26):468–474, January 1959. ISSN 0022-1430, 1727-5652. https://doi.org/10.3189/S0022143000017214. URL https://www.cambridge.org/core/journals/journal-of-glaciology/article/some-preliminary-observations-on-the-plasticity-of-greenland-glaciers/B2A6D22175A910D294916841C931657C.

[104] Jessica M. D. Lundin, C. Max Stevens, Robert Arthern, Christo Buizert, Anais Orsi, Stefan R. M. Ligtenberg, Sebastian B. Simonsen, Evan Cummings, Richard Essery, Will Leahy, Paul Harris, Michiel M. Helsen, and Edwin D. Waddington. Firn Model Intercomparison Experiment (FirnMICE). *Journal of Glaciology*, 63(239):401–422, June 2017. ISSN 0022-1430, 1727-5652. https://doi.org/10.1017/jog.2016.114. URL https://www.cambridge.org/core/journals/journal-of-glaciology/article/firn-model-intercomparison-experiment-firnmice/5146552345761C73763AC80AEB6F7799. Publisher: Cambridge University Press.

[105] Carl S. Benson. *Stratigraphic Studies in the Snow and Firn of the Greenland Ice Sheet. [Hanover, N.H.] U.S. Army Snow, Ice and Permafrost Research Establishment, Corps of Engineers, 1962*. U.S. Department of Commerce, Office of Technical Services, 1963. Google-Books-ID: ttyyZ1rAmm8C.

[106] Don L. Anderson, Carl S. Benson, and W. D. Kingery. The densification and diagenesis of snow. *Ice and snow: properties, processes and applications*, pages 391–411, 1963. URL https://authors.library.caltech.edu/records/jm9c7-3d977/files/Anderson_1963p391.pdf?download=1. Publisher: MIT Press Cambridge, Massachusetts, USA.

[107] J. Besson, F. Valin, P. Lointier, and M. Boncoeur. Densification of titanium diboride by hot isostatic pressing and production of near-net-shape components. *Journal of Materials Engineering and Performance*, 1(5):637–649, October 1992. ISSN 1544-1024. https://doi.org/10.1007/BF02649245. URL https://doi.org/10.1007/BF02649245.

[108] Carlo Scapozza and Perry Bartelt. Triaxial tests on snow at low strain rate. Part II. Constitutive behaviour. *Journal of Glaciology*, 49(164):91–101, January 2003. ISSN 0022-1430, 1727-5652. https://doi.org/10.3189/172756503781830890. URL https://www.cambridge.org/core/journals/journal-of-glaciology/article/triaxial-tests-on-snow-at-low-strain-rate-part-ii-constitutive-40AA9BE110EDC45D5FA2F80290F9190B.

[109] Stefan Schleef, Henning Löwe, and Martin Schneebeli. Hot-pressure sintering of low-density snow analyzed by X-ray microtomography and in situ microcompression. *Acta Materialia*, 71:185–194, June 2014. ISSN 1359-6454. https://doi.org/10.1016/j.actamat.2014.03.004. URL https://www.sciencedirect.com/science/article/pii/S1359645414001475.

[110] J. W. Glen. The Creep of Polycrystalline Ice. *Proceedings of the Royal Society of London Series A*, 228:519–538, March 1955. ISSN 0080-46301364-5021. https://doi.org/10.1098/rspa.1955.0066. URL https://ui.adsabs.harvard.edu/abs/1955RSPSA.228..519G. ADS Bibcode: 1955RSPSA.228..519G.

[111] H.O. K. Kirchner, G. Michot, H. Narita, and T. Suzuki. Snow as a foam of ice: Plasticity, fracture and the brittle-to-ductile transition. *Philosophical Magazine A*, 81(9):2161–2181, September 2001. ISSN 0141-8610. https://doi.org/10.1080/01418610108217141. URL https://doi.org/10.1080/01418610108217141. Publisher: Taylor & Francis _eprint: https://doi.org/10.1080/01418610108217141.

[112] Michael M. Herron and Chester C. Langway Jr. Firn Densification: An Empirical Model. *Journal of Glaciology*, 25 (93):373–385, January 1980. ISSN 0022-1430, 1727-5652. https://doi.org/10.3189/S0022143000015239. URL https://www.cambridge.org/core/journals/journal-of-glaciology/article/firn-densification-an-empirical-model/C9A2B038004A938670B689A6DAE6D89E.

[113] J. M. Barnola, P. Pimienta, D. Raynaud, and Y. S. Korotkevich. CO2-climate relationship as deduced from the Vostok ice core: a re-examination based on new measurements and on a re-evaluation of the air dating. *Tellus B*, 43(2):83–90, 1991. ISSN 1600-0889. https://doi.org/10.1034/j.1600-0889.1991.t01-1-00002.x. URL https://onlinelibrary.wiley.com/doi/abs/10.1034/j.1600-0889.1991.t01-1-00002.x. _eprint: https://onlinelibrary.wiley.com/doi/pdf/10.1034/j.1600-0889.1991.t01-1-00002.x.

[114] C. Goujon, J.-M. Barnola, and C. Ritz. Modeling the densification of polar firn including heat diffusion: Application to close-off characteristics and gas isotopic fractionation for Antarctica and Greenland sites. *Journal of Geophysical Research: Atmospheres*, 108(D24), 2003. ISSN 2156-2202. https://doi.org/10.1029/2002JD003319. URL https://onlinelibrary.wiley.com/doi/abs/10.1029/2002JD003319. _eprint: https://onlinelibrary.wiley.com/doi/pdf/10.1029/2002JD003319.

[115] Andrey N. Salamatin, Vladimir Ya Lipenkov, Jean Marc Barnola, Akira Hori, Paul Duval, and Takeo Hondoh. Snow/firn densification in polar ice sheets. 68(Supplement):195–222, 2009. URL https://scholar.google.com/scholar?cluster=338707491444352175&hl=en&oi=scholarr. Publisher: Institute of Low Temperature Science, Hokkaido University.

[116] C. Max Stevens, David A. Lilien, Howard Conway, T. J. Fudge, Michelle R. Koutnik, and Edwin D. Waddington. A new model of dry firn-densification constrained by continuous strain measurements near South Pole. *Journal of Glaciology*, 69(278):2099–2113, December 2023. ISSN 0022-1430, 1727-5652. https://doi.org/10.1017/jog.2023.87. URL https://www.cambridge.org/core/journals/journal-of-glaciology/article/new-model-of-dry-firndensification-constrained-by-continuous-s-B6DFCA5CED4857F76D7EEA982F538E96.

[117] Henri Bader. Theory of densification of dry snow on high polar glaciers, II. Report, Cold Regions Research and Engineering Laboratory (U.S.), September 1962. URL https://erdc-library.erdc.dren.mil/jspui/handle/11681/5846. Accepted: 2016-03-21T21:08:53Z Publication Title: This Digital Resource was created from scans of the Print

Resource.

[118] Henri Bader. Sorge's Law of Densification of Snow on High Polar Glaciers. *Journal of Glaciology*, 2(15):319–323, January 1954. ISSN 0022-1430, 1727-5652. https://doi.org/10.3189/S0022143000025144. URL https://www.cambridge.org/core/journals/journal-of-glaciology/article/sorges-law-of-densification-of-snow-on-high-polar-glaciers/11F52DA59A607AC2C9ACDC24BEB63156.

[119] R. B. Alley. Firn densification by grain-boundary slidinf: a first model. *Le Journal de Physique Colloques*, 48(C1):C1–256, March 1987. ISSN 0449-1947, 2777-3418. https://doi.org/10.1051/jphyscol:1987135. URL http://dx.doi.org/10.1051/jphyscol:1987135. Publisher: EDP Sciences.

[120] D. L. Goldsby and D. L. Kohlstedt. Grain boundary sliding in fine-grained Ice I. *Scripta Materialia*, 37(9):1399–1406, November 1997. ISSN 1359-6462. https://doi.org/10.1016/S1359-6462(97)00246-7. URL https://www.sciencedirect.com/science/article/pii/S1359646297002467.

[121] Kavitha Sundu, Rafael Ottersberg, Matthias Jaggi, and Henning Löwe. A grain-size driven transition in the deformation mechanism in slow snow compression. *Acta Materialia*, 262:119359, January 2024. ISSN 1359-6454. https://doi.org/10.1016/j.actamat.2023.119359. URL https://www.sciencedirect.com/science/article/pii/S1359645423006894.

[122] M. Ignat and H. J. Frost. GRAIN BOUNDARY SLIDING IN ICE. *Le Journal de Physique Colloques*, 48(C1):C1–189–C1–195, March 1987. ISSN 0449-1947. https://doi.org/10.1051/jphyscol:1987127. URL http://www.edpsciences.org/10.1051/jphyscol:1987127.

[123] J. M. Barnola, D. Raynaud, Y. S. Korotkevich, and C. Lorius. Vostok ice core provides 160,000-year record of atmospheric CO2. *Nature*, 329 (6138):408–414, October 1987. ISSN 1476-4687. https://doi.org/10.1038/329408a0. URL https://www.nature.com/articles/329408a0. Publisher: Nature Publishing Group.

[124] R. J. Arthern and D. J. Wingham. The Natural Fluctuations of Firn Densification and Their Effect on the Geodetic Determination of Ice Sheet Mass Balance. *Climatic Change*, 40(3):605–624, December 1998. ISSN 1573-1480. https://doi.org/10.1023/A:1005320713306. URL https://doi.org/10.1023/A:1005320713306.

[125] Ricardo A. Lebensohn and Oana Cazacu. Effect of single-crystal plastic deformation mechanisms on the dilatational plastic response of porous polycrystals. *International Journal of Solids and Structures*, 49(26): 3838–3852, December 2012. ISSN 00207683. https://doi.org/10.1016/j.ijsolstr.2012.08.019. URL https://linkinghub.elsevier.com/retrieve/pii/S0020768312003642.